

On the dynamics of mortality and the ephemeral nature of mammalian megafauna

Taran Rallings¹, Christopher P Kempes², Justin D. Yeakel^{1,*}

¹*School of Natural Sciences, University of California Merced*

²*Santa Fe Institute*

* *Corresponding author: jyeakel@ucmerced.edu*

Energy flow through consumer-resource interactions is largely determined by body size. Allometric relationships govern the dynamics of populations by impacting rates of reproduction, as well as alternative sources of mortality, which have differential impacts on smaller to larger organisms. Here we derive and investigate the timescales associated with four alternative sources of mortality for terrestrial mammals: mortality from starvation, mortality associated with aging, mortality from consumption by predators, and mortality introduced by anthropogenic subsidized harvest. The incorporation of these allometric relationships into a minimal consumer-resource model illuminates central constraints that may contribute to the structure of mammalian communities. Our framework reveals that while starvation largely impacts smaller-bodied species, the allometry of senescence is expected to be more difficult to observe. In contrast, external predation and subsidized harvest have greater impacts on the populations of larger-bodied species. Moreover, the inclusion of predation mortality reveals mass thresholds for mammalian herbivores, where dynamic instabilities may limit the feasibility of megafaunal populations. We show how these thresholds vary with alternative predator-prey mass relationships, which are not well understood within terrestrial systems. Finally, we use our framework to predict the harvest pressure required to induce mass-specific extinctions, which closely align with previous estimates of anthropogenic megafaunal exploitation in both paleontological and historical contexts. Together our results underscore the tenuous nature of megafaunal populations, and how different sources of mortality may contribute to their ephemeral nature over evolutionary time.

Introduction

Consumer-resource interactions are the fundamental unit from which complex food webs arise [22]. In such dynamics, the rates governing transitions of biomass and energy from one species to another are largely determined by body size [82]. Specifically, the allometric relationships between consumer body mass and metabolic rate constrain energetic assimilation [43], storage [47], and growth [76], all of which govern the dynamics of populations [40, 46, 77, 80]. Because allometrically-constrained models of population dynamics apply generally across large taxonomic clades, they are useful for examining dynamic constraints that may contribute to community structure across macroevolutionary timescales [4, 24, 25, 54, 80]. Furthermore, examination of community dynamics at these scales enables the investigation of extinct communities where body size distributions were different than those in contemporary ecosystems [2, 5, 7].

The dynamics of populations represent an energetic balance between reproduction and mortality [52]. Across Mammalia, the average rate of reproduction can be predicted from allometric scaling relationships [10], though individual clades demonstrate a large variety of reproductive strategies – from changing reproductive cycles, litter sizes, and dynamic responses to changing resource conditions to name a few [61]. As these strategies are typically evolved responses to particular conditions and clade-specific, they are not universally experienced. On the other hand, mortality has a variety of forms that nearly all species must deal with to a greater or lesser extent, and do not all scale similarly with body size

[75]. Mortality originates from both internal and external drivers, where the former depends on an organism’s internal state to initiate death. For example, senescence and starvation involve physiological states that change with respect to clock time, metabolic rate, and resource depletion [60, 80]. In contrast, external drivers of mortality consist of an outside force that induces death more independently of an organism’s internal state, such as mortality due to natural predation or subsidized anthropogenic harvest. Often, mortality occurs through correlations between internal and external drivers, where for example, the starvation state of prey may alter the success rates of predators [1]. While virtually all primary consumer populations must deal with the effects of resource limitation, aging, and predation, the effects of anthropogenic harvesting (the subsidized extraction of prey) are uniquely limited to those species serving as resources for human populations [26].

How do different sources of mortality impact the dynamics of mammalian populations? Here we construct a general consumer-resource framework to examine mammalian herbivore populations as a function of consumer body size M_C , as well as size-dependent vulnerability to different internal and external pressures. Our approach integrates relationships governing specific timescales of physiology and assimilation from a process-based energetic perspective [76]. Our model is low-dimensional and compact [cf. 80], but due to its close connection to fundamental energetic mechanism, it is also capable of reproducing observed large-scale empirical patterns of mammalian communities. We begin by describing our approach, reproducing key macroecological relationships

such as Damuth’s law [20], and examine how changes to energetic parameters impact these predictions. We then derive timescales associated with four sources of mortality experienced by mammalian consumers: *i*) natural mortality, *ii*) starvation mortality, *iii*) natural predation, and *iv*) subsidized anthropogenic harvest. By examining each source of mortality in turn, our framework illuminates central constraints governing mass-specific behaviors, strategies, and risks experienced by mammalian consumers.

Our results reveal four key insights into the constraints structuring mammalian communities. First, our allometric consumer-resource system accurately captures both the central tendency and variability of Damuth’s law, suggesting that the included vital rates capture mass-specific dynamics. Second, our results demonstrate that natural and starvation mortality differentially impact small mammals, confirming expectations, and point to why the allometric effects of senescence are difficult to observe in nature. Third, we detail the differences in how mortality under different levels of predation intensity induce dynamic instabilities for large-bodied megaherbivores. We also show that the body size at which these instabilities occur is dependent on the prevailing predator-prey mass relationship (PPMR). Finally, we evaluate the harvest pressure required to induce mass-specific extinction, and show that our predictions are comparable to estimates of both paleontological and historical exploitation of mammalian megafauna.

Methods

We model a consumer-resource interaction, where the resource R (g/m^2) grows logistically with intrinsic growth rate α to a carrying capacity k , and declines due to consumption by an herbivore consumer population C (g/m^2) (Eq. 3). Consumed resources govern both consumer somatic maintenance and reproduction. The rate of consumption to fuel somatic maintenance is given by ρ , and is independent of resource density, as these are invariant requirements of the consumer population [80]. In contrast, the rate of consumption to fuel reproduction is proportional to resource density and is given by $\lambda_C(R)/Y_C$, where $\lambda_C(R)$ is the consumer growth rate and Y_C is the consumer yield coefficient, or the grams of consumer produced per gram of resource consumed. As in DeLong & Vasseur [25], the consumer’s growth rate $\lambda_C(R)$ follows a Type II (saturating) functional response given the resource density R , where the maximum growth is λ_C^{\max} and the resource half-saturation density is $\hat{k} = k/2$, such that

$$\lambda_C(R) = \lambda_C^{\max} \left(\frac{R}{\hat{k} + R} \right). \quad (1)$$

While the consumer population density grows at rate $\lambda_C(R)$, we assume for now that consumer mortality is a

function of both natural mortality μ and starvation $\sigma(R)$, where the rate of starvation,

$$\sigma(R) = \sigma^{\max} \left(1 - \frac{R}{k} \right), \quad (2)$$

increases as resources become scarce. In this context, σ^{\max} is the maximal rate of starvation that occurs when the environment is devoid of resources. The full system describing resource and consumer dynamics is given by

$$\begin{aligned} \frac{d}{dt}C &= \lambda_C(R)C - (\mu + \sigma(R) + \dots)C, \\ \frac{d}{dt}R &= \alpha R \left(1 - \frac{R}{k} \right) - \left(\frac{\lambda_C(R)}{Y_C} + \rho \right)C, \end{aligned} \quad (3)$$

where the ‘...’ denotes where additional mortality terms, described later, will be included. The dynamic outcomes of this system of equations include two trivial steady states at $(R^* = 0, C^* = 0)$ and $(R^* = k, C^* = 0)$, and one internal steady state where both the consumer and resource population coexist. See tab. I for a description of parameters.

The rate laws describing resource consumption as well as consumer growth and mortality all vary as a function of consumer body mass M_C , where the consumer is assumed to be a mammalian herbivore, and the resource is an unspecified primary producer with characteristic growth rate, carrying capacity, and energy density E_d . We approach the derivation of vital rates with respect to consumer mass by solving for multiple timescales associated with ontogenetic growth, maintenance, and expenditure. The growth of an individual consumer from birth mass $m = m_0$ to its reproductive size $m = 0.95M_C$ is given by the solution to the general balance condition $B_0m^\eta = E_m \frac{d}{dt}m + B_m m$, where E_m is the energy needed to synthesize a unit of biomass, B_m is the metabolic rate to support an existing unit of biomass (tab. I), and the metabolic exponent $\eta = 3/4$ [43, 56, 76]. From this balance condition, the time required for an organism starting from mass m_1 to reach mass m_2 follows

$$\tau(m_1, m_2) = \ln \left(\frac{1 - (m_1/M_C)^{1-\eta}}{1 - (m_2/M_C)^{1-\eta}} \right) \frac{M_C^{1-\eta}}{a(1-\eta)} \quad (4)$$

where $a = B_0/E_m$ [76]. We use this general timescale equation to calculate maximal rates of growth and starvation as a function of organismal body size M_C , which are then modified by resource density R to provide realized timescales (eqs. 1,2). We note that a more complex framework could include the effects of changing resource densities on timescales directly, where individual growth is itself variable, effectively introducing dynamic population structure [21]. From this general equation, we calculate the timescale of reproduction for an herbivore consumer of mass M_C as $t_{\lambda_C} = \tau(m_0, 0.95M_C)$, such that the maximal reproductive rate is $\lambda_C^{\max} = \ln(\nu)/t_{\lambda_C}$, where $\nu = 2$ is the set number of offspring per reproductive cycle [63, 80]. The consumer yield coefficient is

given by $Y_C = M_C E_d / B_{\lambda_C}$ (g consumer per g resource), where B_{λ_C} is the lifetime energy use required by the herbivore to reach maturity $B_{\lambda_C} = \int_0^{t_{\lambda_C}} B_0 m(t)^\eta dt$, and the maintenance rate is given by $\rho = B_0 M_C^\eta / M_C E_d$ [80].

To determine the rate of mortality from starvation, we calculate the time required for an organism to metabolize its endogenous energetic stores, estimated from its cumulative fat and muscle mass, where the remaining mass is given by $M_C^{\text{starve}} = M_C - (M_C^{\text{fat}} + M_C^{\text{musc}})$ (see app. C). During starvation, we assume that an organism burns its existing endogenous stores as its sole energy source, such that the balance condition is altered to $\frac{d}{dt} m E'_m = -B_m m$, where E'_m is the amount of energy stored in a unit of biomass (differing from the amount of energy used to synthesize a unit of biomass E_m ; tab. I) [43, 51]. The starvation timescale is then given by

$$t_\sigma = -\frac{M_C^{1-\eta}}{a'} \ln(M_C^{\text{starve}}/M_C), \quad (5)$$

where $a' = B_0/E'_m$, such that the starvation rate is the $\sigma^{\text{max}} = 1/t_\sigma$. Importantly, the starvation mortality expressed here is specifically that experienced by adult organisms (as the timescale of metabolizing fat stores is conditioned on adult mass), and does not capture potential starvation mortality of juveniles.

To determine the rate of mortality from aging, we note that population cohorts experience two primary sources of natural mortality: the initial cohort mortality rate q_0 and the annual rate of increase in mortality as the cohort ages, or the actuarial aging rate, q_a over lifetime t_ℓ . We begin by assuming that the number of survivors over time follows a Gompertz relationship [10] from which we derive the average rate of natural mortality

$$\mu = \frac{q_0}{q_a t_\ell} (\exp(q_a t_\ell) - 1). \quad (6)$$

The three parameters (q_0, q_a, t_ℓ) each have well-documented allometric relationships for terrestrial mammals, such that natural mortality can be written as a function of consumer mass $\mu(M_C)$ (see app. A). Because both cohort and actuarial mortality are not subdivided into specific categories, we may assume that this rate is capturing the combined effects of all sources of mortality, particularly during early development when starvation and predation risks are highest.

As the sizes of physiological biomass compartments are obtained from empirical observations, the rates determining biomass flux are derived from process-based energetic relationships (eq. 4). Together, the allometric rate laws and the dynamic system presented in Eq. 3 allow us to assess the dynamics of consumer-resource systems for mammalian herbivores spanning the observed range of terrestrial body sizes, from the smallest (the Etruscan shrew at roughly 1 g) to the largest (the Oligocene paraceratheres and Miocene deinotheres at ca. $1.5 - 1.74 \times 10^7$ g) [67]. We next examine how this minimal framework is well-suited to provide general insight into several key

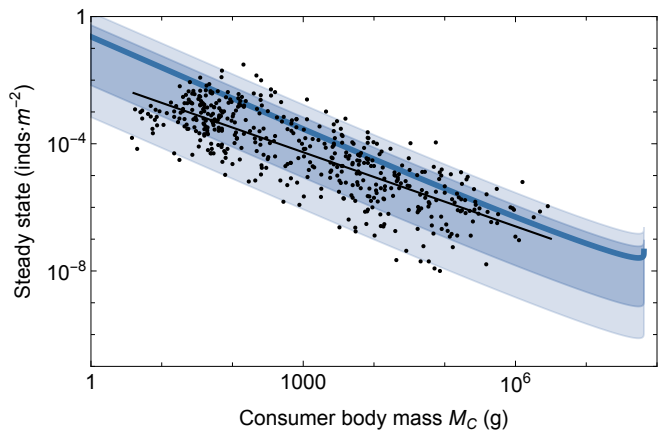


Figure 1: Model predictions of mammalian steady states ($\text{inds} \cdot \text{m}^{-2}$) as a function of herbivore consumer body mass M_C (thick blue line) compared to observational data from Damuth [20] (black points). The black line denotes the best-fit linear regression on observed densities based on ordinary least squares. Variation in steady state densities is captured by allowing the plant resource growth rate to vary as $\alpha = 2.81 \times 10^{-10} : 2.19 \times 10^{-8} \text{ s}^{-1}$ (dark blue shaded region), and both α and the plant resource carrying capacity to vary as $k = 2.3 : 34 \text{ kg/m}^2$ (light blue shaded region).

allometric constraints that contribute to the functioning and limitations of terrestrial mammalian communities.

Results & Discussion

Recovering Damuth's mass-density relationship

Our consumer-resource system is related to the nutritional state model (NSM) proposed in Yeakel et al. [80], where an explicit starvation dynamic was incorporated by separating the consumer population density into 'full' and 'hungry' states. Here we eliminate the transition between these states, and because the timescales of transitioning between full and hungry states are short relative to those of reproduction, have sacrificed only a modest degree of physiological realism to enable analytical expression of steady states with additional sources of mortality. If we ignore the negligible effects of ρ (see app. B), analytical expression of the consumer steady state as a function of mass – or the mass-density relationship – follows

$$C^*(M_C) \approx \alpha k Y_C \frac{\sigma^{\text{max}} - 2\lambda_C^{\text{max}} + A}{4\sigma^{\text{max}2}}, \quad (7)$$

where $A = \sqrt{8\sigma^{\text{max}2} + (\sigma^{\text{max}} - 2\lambda_C^{\text{max}})}$, where λ_C^{max} , σ^{max} and Y_C are functions of mass M_C .

The scaling of mammalian population densities was originally observed by Damuth [18, 19] as the reciprocal

of energy use requirements with an exponent of ca. $-3/4$. Consumer-resource models parameterized using allometric relationships can effectively predict this mass-density relationship [25, 80, 82], while the addition of predator-prey size ratios and consumer capture relationships enable similar predictions at higher trophic levels [24, 75]. By integrating dimensional scaling into search and consumption rates, Pawar et al. [54] captured the mass-density relationship while highlighting potential instabilities arising in 3-Dimensional (aquatic) environments. Our approach differs from most prior efforts by deriving timescales associated with reproduction and mortality directly from the energetic trade-offs associated with somatic growth and maintenance. After substituting allometric relationships into the rate laws in Eq. 3, we observe that the internal steady state of consumer densities in our framework is very close, though slightly elevated, to observed mammalian densities, similarly approximating Damuth's Law (blue line, fig. 1).

Our predicted mass-density relationship is premised on the assumption of resource growth rates and carrying capacities characteristic of grasses (tab. I), contributing to the slightly elevated mass-density relationship compared to the observed best-fit (black line, fig. 1). As the resource growth rate and carrying capacity are in the numerator of eq. 7, they determine the intercept of the relationship such that lower values will more closely match observed densities. Along these lines, incorporating observed ranges of α and k reveal strong alignment between model predictions and the variability of empirical mammalian densities (fig. 1; see app. B for details). Compared to the NSM [80], and similar to DeLong and Vasseur [24], our prediction reveals exaggerated densities for smaller-bodied consumers, though within the observed range of variation, resulting in a predicted mass-density relationship with a steeper slope than expected. An elevated mass-density slope is not observed when explicit starvation and recovery are included [80], suggesting these dynamics play an important role in depressing the populations of smaller-bodied species, in particular.

While eq. 7 cannot be readily expressed when allometric relationships are included, for larger body sizes the maximal starvation rate $\sigma^{\max} \propto M_C^{-0.3}$, the yield coefficient $Y_C \propto M_C^{-1/4}$, the maximal consumer growth rate $\lambda_C^{\max} \propto M_C^{-1/4}$, and the quantity $A \propto M_C^{-0.37}$. For larger body masses, this results in a predicted mass-density relationship $\propto M_C^{-0.82}$ inds/m², only slightly steeper than Damuth's mass-density relationship $\propto M_C^{-0.77}$ inds/m². At unrealistically large body sizes, the consumer steady state encounters a vertical asymptote [also noted in 80]. In this region, the superlinear body fat allometry (tab. I) predicts the organism to be 100% fat, such that the starvation timescale is infinite. While this is mathematically entertaining, we restrict our interpretations to realistic body size ranges, thereby avoiding this particular physiological singularity. We examine additional effects of altered vital rates on the slope and intercept of the

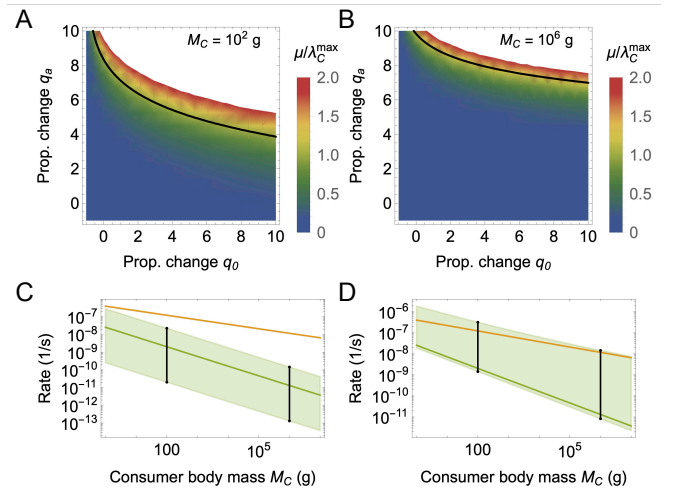


Figure 2: Changes in natural mortality as a function of initial cohort mortality q_0 , and actuarial aging, q_a for two different consumer body masses, M_C . A,B. The ratio reproduction λ_C^{\max} to natural mortality μ for a mammalian herbivore of A. $M_C = 10^2$ g and B. $M_C = 10^6$ g, across proportional changes to the initial cohort mortality rate q_0 and the actuarial aging rate q_a . The black contour denotes $\mu/\lambda = 1$. C,D. Natural mortality μ (green) relative to reproduction λ_C^{\max} (orange) as a function of consumer body mass M_C . The range of variation (light green shaded region) shows proportional changes to the C. cohort mortality rate q_0 and the D. actuarial aging rate q_a from -0.99 to 10 .

mass-density relationship in app. B.

Senescence and starvation have a larger impact on smaller consumers

We first consider two internal sources of mortality: that due to the effects of aging, where mortality changes with an organism's temporal state, and that due to starvation, where mortality scales with an organism's energetic state. To understand the effect of changes to $\mu(M_C)$ on consumer steady states, we examine variations in the principle components of μ : initial cohort mortality q_0 and actuarial mortality q_a . The initial cohort mortality represents the mortality experienced by a cohort prior to accruing effects of age. We observe that the mortality rate changes proportionally with q_0 independent of consumer mass, where the ratio $\mu/\lambda_C^{\max} < 1$ even with respect to large increases in q_0 , unless q_a is similarly magnified (fig. 2A,B). For survivorship mortality to approach the rate of reproduction ($\mu/\lambda_C^{\max} = 1$), where perceptible declines in population densities result, the initial cohort mortality must increase by roughly an order of magnitude (shaded region in fig. 2C). Due to the steepness of the scaling of μ relative to λ_C^{\max} , this effect is felt exclusively by small-bodied organisms.

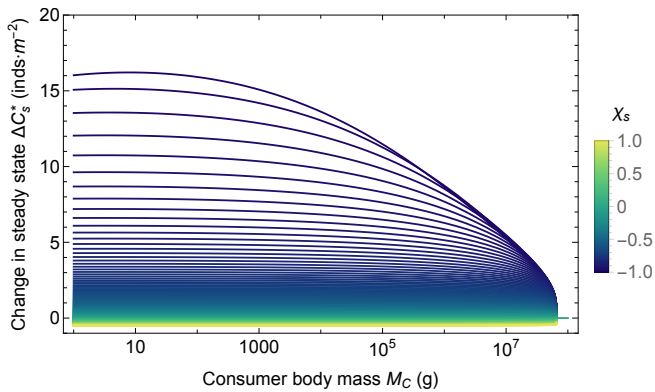


Figure 3: The relative change in consumer steady state ΔC_s^* as a function of consumer body mass M_C given an altered rate of starvation $\sigma(R) \cdot (1 + \chi_s)$ across the proportional change $\chi_s \in (-0.99, 1)$.

Actuarial mortality represents the cumulative effects of aging, or senescence, across the organism’s expected lifetime. We observe that as q_a increases, the magnitude of mortality increases disproportionately (fig. 2A,B), while the slope of $\mu(M_C)$ becomes more shallow (fig. 2D), primarily due to the cumulative nature of senescence magnifying its effects across the longer lifetimes of larger mammals. As such, an increase in q_a overwhelms reproduction such that $\mu/\lambda_C^{\max} > 1$, resulting in population instability (fig. 2A,B). The extinction risk imposed by senescence has been explored across mammalian taxa, and while some life-history characteristics such as the inter-birth interval appear to correlate strongly with these risks, the role of body size is notably ambiguous [60]. Though our model – which considers averaged effects across terrestrial mammals – predicts that the risks of increased actuarial mortality are disproportionately felt by smaller size-classes, we also show that $\mu(M_C)$ increasingly resembles $\lambda_C^{\max}(M_C)$ with increasing q_a (the top border of the shaded region in fig. 2D). This increased similarity implies that relatively small variations in other demographic processes or interactions may have potentially large and destabilizing effects on population size that cannot be predicted from body mass, a potential source for the noted ambiguity between size and actuarial extinction risk [60].

While the temporal state of an organism is unidirectional and linear, other internal states, such as an organism’s energetic state, fluctuate nonlinearly over time. In this case, the rate of starvation is low when resources become plentiful ($R \rightarrow k$) and increases to σ^{\max} as resources become scarce ($R \rightarrow 0$). Because organisms metabolize their fat and muscle tissue during starvation, and die from starvation when these energetic stores are metabolized, the timescale of starvation varies with the amount of endogenous energetic stores an organism carries. Larger organisms carry a larger proportion of body mass as fat [47], such that they are more protected from the effects of short-term resource scarcity [49]. We ob-

serve this effect by modifying the starvation rate and examining how the steady state population size is altered. We introduce variation to the rate of starvation as $\sigma(R) \cdot (1 + \chi_s)$, from which the altered steady state C_s^* is calculated. The relative change in steady states introduced by the altered starvation rate is then given by $\Delta C_s^* = (C_s^* - C^*)/C^*$, where positive values indicate a relative gain in steady state densities from the proportional change χ_s , and negative values indicate a relative loss (fig. 3). We observe that, while all mammals benefit from reduced starvation rates ($\chi_s < 0$), smaller-bodied mammals benefit to a much greater extent, and this effect tapers off with increasing body mass. Because fat biomass scales super-linearly with body mass, the populations of larger consumers are more resilient to the effects of starvation, whereas those of smaller consumers are more prone.

An organism’s rate of starvation emerges from two governing forces – the amount of energy storage and the rate of its use – and as such can be manipulated both physiologically and behaviorally. For instance, behaviorally supplementing endogenous fat stores with exogenous caches magnifies an individual’s energetic stores [48, 79], whereas physiologically-mediated responses to starvation risk such as torpor can introduce significant temporal delays to the effects of resource scarcity [64]. In both cases the time required to pass from a replenished to a starved state is effectively increased, lowering the rate of starvation. The predicted benefits of such adaptations to mammalian steady state densities will be realized primarily by smaller mammals (fig. 3, app. B), and it is the smaller body size range where traits such as caching and torpor are most commonly observed [31, 66, 79].

Predation mortality and the feasibility of megatrophic interactions

Predators introduce an external source of mortality on prey populations, fueling their own population growth in whole (trophic specialists) or in part (trophic generalists), by the rate at which prey are consumed. We account for the effects of an implicit predator density P with body size M_P on the herbivore consumer density C with body size M_C , where we assume the predator population to exist at a fixed density $P \equiv P^*$. The mortality rate of the herbivore consumer from an external predator is given by

$$\beta(C, P) = w \frac{\lambda_P(C)P}{CY_P}, \quad (8)$$

where $\lambda_P(C)$ is the growth rate of the predator and Y_P is the predator yield coefficient, describing the grams of predator produced per gram of prey consumed, and w is the predation intensity. Mirroring the calculation of the consumer yield coefficient, $Y_P = M_C E_C / B_{\lambda_P}$, where E_C is the energy density of consumable biomass carried

by herbivore prey, and the B_{λ_P} is the lifetime energy requirement of the predator (app. C).

Assuming a linear functional response for predation mortality, $\lambda_P(C)$ is maximized when the consumer reaches its theoretical maximum population density, which we calculate by converting the resource carrying capacity directly to grams of consumer produced, or $C^{\max} = Y_C k$. While this is an ultimately unattainable theoretical bound, it allows for a direct calculation of the predator growth rate as a function of C , written as

$$\lambda_P(C) = \lambda_P^{\max} \frac{C}{C^{\max}} = \lambda_P^{\max} \frac{C}{Y_C k}, \quad (9)$$

where $\lambda_P^{\max} = \ln(\nu)/t_{\lambda_P}$ is the maximum predator growth rate, given $\nu = 2$, and t_{λ_P} is the time required for the predator to reach maturity (following eq. 4). The theoretical boundary density for herbivore consumers C^{\max} can similarly be used to calculate the boundary density for predators, $P^{\max} = Y_P C^{\max}$, both of which accurately capture the upper-bounds of herbivore and carnivore mass-density observations (dashed lines in fig. 4A). Because the effects of the predator are implicit, we assume that the predator population remains at empirically measured steady state densities for mammalian carnivores, where $P^* = p_0 M_P^{p_1}$ given $p_0 = 8.62 \times 10^{-4}$ inds $^{1-p_1}$ /m 2 and $p_1 = -0.88$ [11]. As we are employing this framework to evaluate longer-term evolutionary consequences, this condition assumes that predator densities do not have long-term feasibility if they stray far from P^* .

The predation mortality rate depends on both the body size of the herbivore consumer and its respective predator. Trophic interactions are constrained by body size [8, 33, 65], though the nature of the predator-prey mass relationship (PPMR) varies across communities [3] and size classes [8, 12, 53, 55, 58, 62]. Compellingly, PPMRs for many clades can be predicted from the scaling of handling time [23], suggesting that the signatures of body size evolution has cascading effects on community structure and function. While prior work has largely focused on the expected prey mass for a given predator mass, because our framework is prey-centric we require a prediction of the expected predator mass M_P given an herbivore of body size M_C . For larger predators and prey ($> 10^5$ g), the expected predator mass given a particular herbivore mass follows roughly $E\{M_P\} = v_0 M_C^{v_1}$, where $v_0 = 9.76 \times 10^3$ g $^{1-v_1}$ and $v_1 = 0.21$ [fig. 4B; see app. C; 34–39]. [Here and throughout the prefix ‘mega’ is used to signify size classes $> 5 \times 10^5$ g; 38]. Accordingly, larger terrestrial herbivores tend to suffer mortality from proportionately smaller predators, an asymmetry that becomes more pronounced with increasing size [cf. 65]. We note that smaller terrestrial predator/prey size classes tend to be much larger than prey [e.g. rodent- or insect-specialist mesocarnivores; 16, 17], also captured by the $E\{M_P\}$ scaling.

Integrating the large-bodied PPMR into the predation mortality rate reveals the emergence of a dynamic in-

stability at megaherbivore size classes (fig. 4A,B), the product of a transcritical bifurcation at consumer mass M_C^\dagger (app. C), and similar to the more general instability documented by Weitz and Levin [75]. An implicit predator population with body size $E\{M_P\}$ is thus able to withdraw sufficient biomass from an herbivore population – without crashing the herbivore population – below a threshold herbivore size of $M_C^\dagger = 2.58 \times 10^6$ g (fig. 4A). Above this critical size threshold, the herbivore population has such low densities that it is unable to sustain a specialist predator species large enough to consume it, introducing a strong upper-bound to mammalian carnivore body size driven by a trophic cascade. This boundary matches the herbivore maximum size limit observed in contemporary terrestrial systems [65], at roughly the size of an elephant (fig. 4B; app. C), though the exact placement of M_C^\dagger varies with the resource growth rate and carrying capacity. While we have assumed values representative of grass resources, decreasing α and/or k lowers the steady state mass-density intercept (eq. 7), setting the mass threshold at a lower body size (app. C). This means that lower-productivity environments, or environments subject to large and long-term oscillations in productivity, may be expected to have more severe limitations on feasible megaherbivore sizes. And while we do not consider stochastic or transient effects directly, we may also assume actualized extinction risk to emerge at smaller-than-predicted masses where transient or stochastic effects may push populations below the point of recovery.

M_C^\dagger marks the threshold herbivore mass above which predation is unsustainable, though Sinclair et al. [65] revealed contemporary herbivores to escape predation at ca. 4.22×10^5 g. This change-point reflects the limitations of contemporary carnivores, which reach a maximum body size of 1.15 to 2.60×10^5 g [65], and have preferences for prey up to 5.50×10^5 g [38]. Importantly, the sole predators of contemporary giants are not megaherbivore specialists, instead opportunistically subsidizing their preferred prey with larger taxa. While we have so far assumed a predator-prey interaction where the entirety of predator growth is fueled by the focal herbivore, the largest predators in natural systems tend to be dietary generalists [32, 65]. We observe that reducing the predation intensity (such that $w < 1$) increases M_C^\dagger to a larger threshold mass (app. C). For example, $w = 0.37$ increases the herbivore body mass boundary to $M_C^\dagger = 1.75 \times 10^7$ g (fig. 4B; app. C), roughly the body mass attained by the largest terrestrial herbivores, the Oligocene paraceratheres and Miocene deinotheres [67].

That the threshold herbivore mass decreases with increasing predation intensity suggests that larger predators are dynamically constrained to be dietary generalists [65], while also pointing to an amplifying feedback mechanism [7] that may operate in diverse communities undergoing megafaunal extinctions. As megaherbivore species are lost, the largest predators must respond by

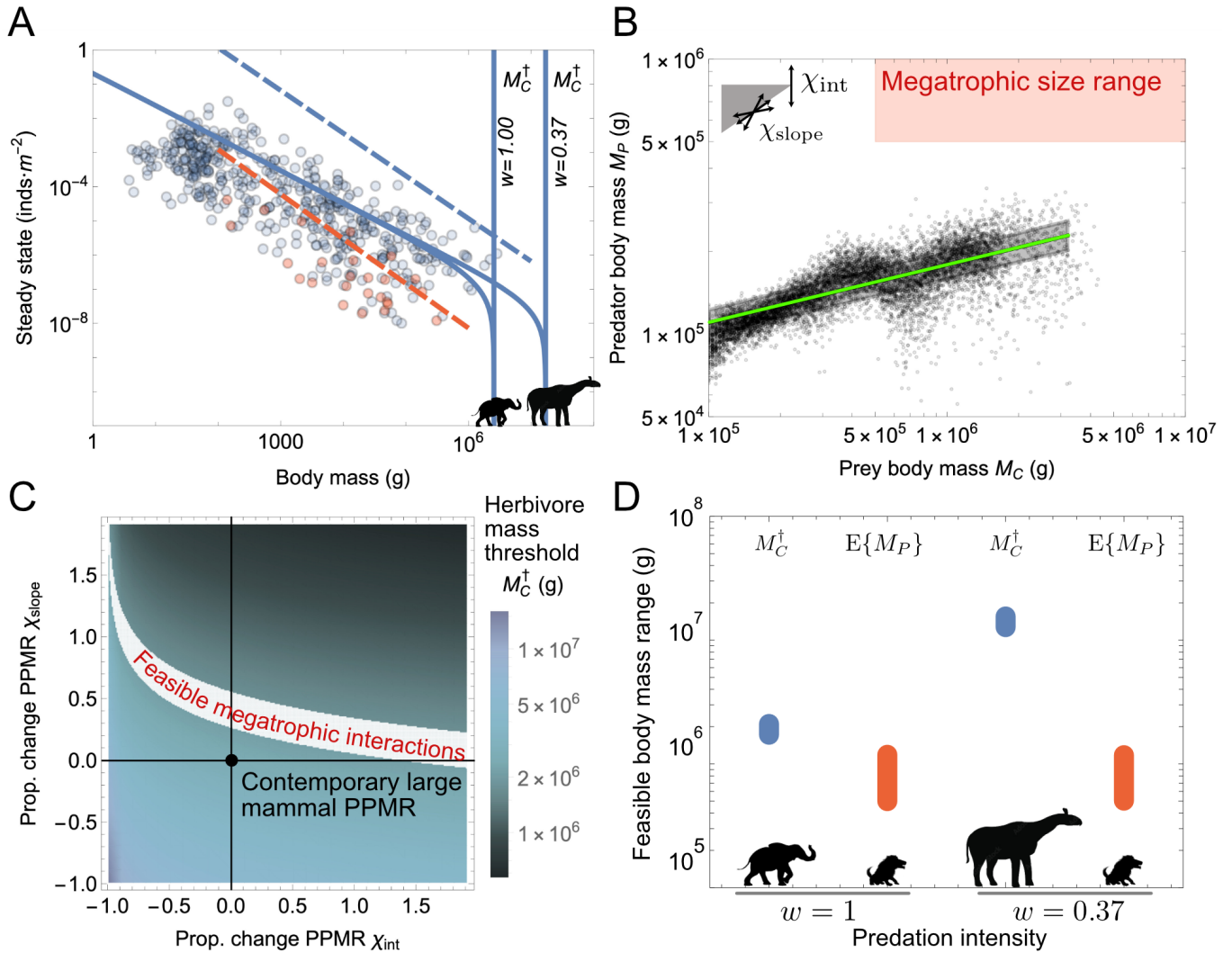


Figure 4: The feasibility of predation. A. Empirical mammalian herbivore (blue points) and predator (red points) mass-densities shown alongside the theoretical maximum herbivore C^{\max} and predator P^{\max} densities across body size (dashed lines). The solid blue curves denote the predicted herbivore consumer steady state $C^*(M_C)$ with predation mortality given high ($w = 1$) and low ($w = 0.37$) predation intensities. B. Predator body mass as a function of prey body mass observed among contemporary mammalian fauna provides the allometric predator-prey mass relationship (PPMR). The green line denotes the best-fit, where $M_P = 9.76 \times 10^3 M_C^{0.21}$ g. C. Threshold herbivore mass M_C^\dagger given changes to the PPMR intercept χ_{int} and slope χ_{slope} (see Eq. A25 and legend in B.). White shaded region highlights the mass range enabling feasible megatrophic interactions, shown in D. for herbivore mass thresholds M_C^\dagger with the expected mass of associated carnivores $E\{M_P\}$, assuming alternative predation intensities.

increasing the intensity of predation on those remaining. Our results suggest that this energetic redirection reduces the threshold herbivore mass M_C^\dagger to lower size classes, increasing the likelihood of additional extinctions and attendant increases in predation intensity on survivors. Together, this demonstrates a dynamic mechanism for the previously proposed influence of top-down dietary ratcheting hypothesized for the Pleistocene extinctions, in particular [45, 59].

Adaptations to hypercarnivorous strategies are diffi-

cult to reverse on macroevolutionary time scales, resulting in the so-called ‘hypercarnivore ratchet’ [41, 71]. Moreover, there is a strong correlation between hypercarnivorous adaptations and body size among terrestrial carnivores, the combination of which may promote vulnerability to extinction [72]. While deinotheres and paraceratheres top the megaherbivore scale, the Eocene artiodactyl *Andrewsarchus* may have been the largest terrestrial mammalian predator at ca. 1×10^6 g [9], while the Miocene Hyaenodontid *Megistotherium osteoth-*

lastes ranged between 5 to 8×10^5 g and the early Eocene Oxyaenodont *Sarkastodon mongoliensis* weighed ca. 8×10^5 g [69]. A theoretical maximum mammalian carnivore size of 1.1×10^6 g has been proposed based on the intersection of daily energetic uptake requirements against metabolic expenditures [13], closely aligning with the largest known megapredators. While our consumer-resource framework provides a range of predicted megaherbivore body mass thresholds depending on the fraction of predator growth it fuels, we next ask under what conditions megatrophic relationships between megaherbivores and megapredators are dynamically feasible.

A central relationship in our framework is the allometric PPMR observed for the largest contemporary herbivores and carnivores, however empirical observations of PPMRs reveal tremendous variability both across and within clades [23], and are completely unknown for megatrophic interactions in terrestrial systems (fig. 4B; app. C). While it is unknown whether these super-sized carnivores were specialists on deinotheres size-classes, our framework allows us to investigate whether and to what extent changes to the contemporary PPMR enable megatrophic interactions (fig. 4C,D). To examine this, we allow the expected predator mass given a particular prey mass to vary as

$$E\{M_P\} = v_0(1 + \chi_{\text{int}})M_C^{v_1(1+\chi_{\text{slope}})}, \quad (10)$$

where the proportional changes in the PPMR intercept and slope are given by χ_{int} and $\chi_{\text{slope}} \in (-0.99, 2)$ (see the legend in fig. 4B). We note that while χ_{slope} explores changes to the inferred steepness of the PPMR, χ_{int} explores variation around the scaling relationship for a particular prey mass.

We observe that only a small range of values for PPMR intercepts and slopes permit the existence of dynamically feasible megatrophic interactions, where megaherbivores serve as prey for specialized megapredators (white band in fig. 4C,D; app. C). Such interactions could be realized if the PPMR in fig. 4B had an increased intercept or alternatively both a lower intercept and higher slope for mega size-classes. That alternative PPMRs could characterize different size-classes across foraging guilds has been previously examined [12, 73], and the clear disconnect between that shown for contemporary large-bodied mammals and those in the megatrophic range (fig. 4B) supports this notion. When predation intensity is high ($w = 1$), the PPMR enabling feasible megatrophic interactions lowers the herbivore mass threshold M_C^\dagger , resulting in megapredators consuming relatively smaller prey. However, if predation intensity is lowered ($w = 0.37$), we observe feasible megatrophic interactions for size-classes capturing megaherbivores and megapredators at their largest documented sizes in the fossil record (fig. 4D; app. C).

That decreased predation intensity enables feasibility of the largest mammalian size-classes agrees with previous conjectures that the largest mammalian terrestrial

predators were likely dietary generalists [29]. Our framework thus highlights dynamic constraints existing between predators and prey that may serve to structure mammalian communities over evolutionary time, in particular revealing the susceptibility of megaherbivores to perturbations. As carnivorous clades evolved body sizes enabling megaherbivore predation, their super-sized appetites may have suppressed megaherbivores to unsustainable densities where the risk of extinction became overwhelming – an evolutionary trap marking the final tooth in the hypercarnivore ratchet [cf. 72].

Harvesting to extinction

We last consider the effects of anthropogenic harvest-induced mortality on herbivore populations. While the predation rate is naturally limited by the energetic needs of the predator, we consider harvest to be a comparatively unconstrained source of mortality. This may be the case if the human population(s) engaged in harvesting are subsidized by alternative resources [6]. Harvest pressure has potentially varying relationships with consumer (prey) body mass, a complex product of environment, climate, culture, and technology [15]. For example, hunting traditions specializing in mass-collecting, by way of trapping or netting [15, 70] are expected to exhibit harvest allometries biased towards smaller species, whereas a purely opportunistic strategy may be expected to have very little allometric dependence. While smaller mammals do not appear to offer a significant return on investment, the mass-collecting of invertebrates, such as grasshoppers, and fish can offer significant returns [70]. In contrast, the innovation of advanced projectiles is thought to have enabled harvest of terrestrial megafauna [15, 57], and archeological evidence points to many Pleistocene human populations as potential megafaunal specialists [68].

Because harvest scaling may be difficult to measure and idiosyncratic, we instead calculate the harvest rate required to induce extinction, h^\dagger , as a function of body size M_C , and find a scaling relationship proportional to the rate of reproduction where $h^\dagger \propto M_C^{-1/4}$. This is a natural result, as the effort required to suppress a population is expected to be proportional to its reproductive rate, reflecting the increased susceptibility of large-bodied organisms to extinction [27]. As a proportion of the other sources of consumer mortality that we have considered (excluding predation; $w = 0$), extinction-level harvesting is lower for smaller consumers, saturating at close to unity at large size classes, reflecting the elevated role of starvation mortality among smaller-sized organisms (Fig 5A). With predation mortality included at both low ($w = 0.37$) and high ($w = 1$) intensities, extinction-level harvesting accounts for an increasingly smaller proportion of mortality for larger organisms (orange and red lines, fig. 5A). This highlights the delicate nature of the megafaunal niche, where smaller changes in

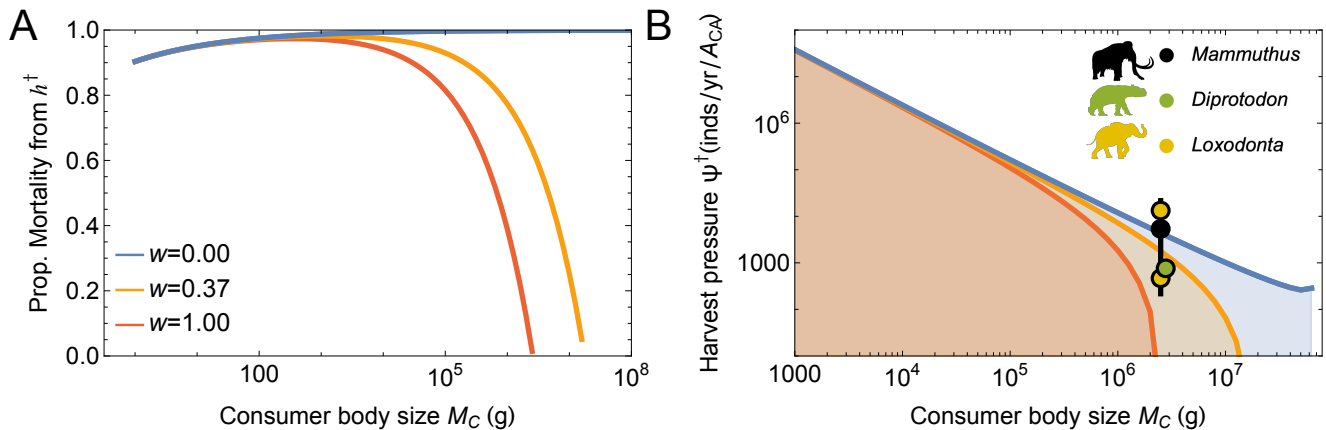


Figure 5: The effects of harvest mortality on herbivore consumers. A. Proportion mortality due to an extinction-inducing harvest rate h^\dagger without predation ($w = 0$; blue line), and with low ($w = 0.37$; orange line) or high predation intensity ($w = 1$; red line), as a function of consumer body mass M_C . B. Harvest pressure ψ^\dagger resulting from extinction-inducing harvest (inds/year/ A_{CA}) without predation ($w = 0$; blue line), and with low ($w = 0.37$; orange line) or high predation intensity ($w = 1$; red line), as a function of consumer body mass M_C . Black point and line: median and range of estimated harvest rates for woolly mammoths [*Mammuthus primigenius*; 30]; Green point: estimated harvest pressure for the Australian *Diprotodon* [5]; lower and higher yellow point: estimated harvest rates for contemporary *Loxodonta* during the early 1800s and just prior to 1987, respectively [50].

mortality rates can induce population collapse [27].

To examine how our estimate of extinction-level harvesting rates h^\dagger compare to those estimated for human hunting of paleontological and historical mammalian populations, we converted h^\dagger to harvest pressure ψ^\dagger , or the number of individuals harvested per year to reduce the population to a fraction of its steady state ϵC^* where we set $\epsilon = 0.01$. We calculate ψ^\dagger for an arbitrary area (see app. D), which we standardize to the area of California ($A_{CA} = 4.24 \times 10^5 \text{ km}^2$), such that

$$\psi^\dagger \propto -h^\dagger \frac{C^*(1-\epsilon)}{M_C \log(\epsilon)}. \quad (11)$$

Though the annual harvesting pressure is unrealistically high for smaller organisms, we observe that it is ca. $4.3 \times 10^3 \text{ inds/yr}/A_{CA}$ for elephant-sized mammals (ca. $2.5 \times 10^6 \text{ g}$) in the absence of predation mortality ($w = 0$). With increasing predation intensity, the harvest pressure required to induce extinction is much less for these larger consumers (orange and red lines in fig. 5B). We note that this calculation of harvest pressure should be viewed as a minimum estimate given that we do not account for demographic rebound. As such, this measure is appropriate only if the timescale of harvest is less than the generational timescale, which is the case for the megafauna considered here.

Our predictions of extinction-inducing harvest pressure compare well with paleontological and historical estimates of harvest pressure on mammalian megafauna (fig. 5B; see app. D). For example, using a formulation similar to that of Alroy [2], Fordham et al. [30] estimate the harvest pressure required to collapse mammoth (*Mammuthus primigenius*) populations, revealing a

range of values consistent with our expectation for similar size-classes (est. $\psi^\dagger = \text{ca. } 1.24 \times 10^4 \text{ inds/yr}/A_{CA}$), as did estimates of extinction-inducing harvest of the Australian *Diprotodon* [est. $\psi^\dagger = \text{ca. } 763 \text{ inds/yr}/A_{CA}$; 5]. Within the historical record, elephant (*Loxodonta*) populations experienced comparatively lower harvest pressure through 1850 [ca. $466 \text{ inds/yr}/A_{CA}$, derived from the volume of ivory exports; 50]. While fluctuating over the next century, harvest pressure increased to a maximum of ca. $13.3 \times 10^5 \text{ inds/yr}/A_{CA}$ just prior to 1987 (fig. 5B). This level of harvest was not sustained, as ivory export volume plummeted following the implementation of trade restrictions in 1989 [50]. Both the Fordham et al. [30] estimate for Pleistocene mammoths and the short-lived harvest maximum for African elephants in 1987 [50] achieved pressures greater than ψ^\dagger under the conservative assumption of no natural predation (fig. 5B). While estimates for *Diprotodon* harvest are considerably lower [5], it is important to note that our framework is parameterized for eutherian rather than marsupial mammals. Nevertheless, the estimated *Diprotodon* ψ^\dagger is well within range of extinction-inducing harvest rates if natural predation pressures are also included, and there is evidence to suggest that *Diprotodon* likely served as prey for marsupial lions [42, 78], and both giant crocodylians (*Pallimnarchus* spp.) and varanid lizards [*Megalania* spp.; 74].

Conclusion

We have shown that the inclusion of mass-specific energetic transfer between resources and consumers, com-

bined with the unique timescales governing consumer mortality, both predict Damuth’s Law [20] and provide insight into dynamic thresholds constraining populations. While natural and starvation mortality primarily impact small-bodied species, trophic mortality primarily impacts large-bodied species with longer generational timescales. Moreover, while mass-specific predation gives rise to dynamic thresholds for herbivore populations, these effects are sensitive to both predation intensity as well as the associated predator-prey mass relationship, which isn’t well understood in terrestrial ecosystems [53]. While assessment of particular communities and/or species requires more detailed approaches – integrating, for example, life history dynamics as in Bradshaw et al. [5] – we suggest that a lower-dimensional framework is useful for extracting general, first-order energetic constraints that both shape and potentially limit the nature of mammalian communities.

That extinction risk appears to increase with body size [14] is integral to our understanding of the Pleistocene extinctions [2, 5, 7, 44, 68] and anthropogenic effects throughout the Holocene [28]. Because megafaunal loss may have disproportionately large impacts on ecosystem functioning [27], understanding the mechanistic drivers that may lead these species to the brink is of paramount importance. Assessing which energetic walls close in and why as body size increases, is a fundamental aspect of reconciling the nature of extinction [7], particularly when there is size-selectivity [68]. That we observe dynamically-feasible megatrophic interactions to occupy a narrow band of predator-prey mass relationships points to a broader range of interaction structures than are realized in contemporary communities. As the threshold consumer mass decreases with increased predation in-

tensity, how megafaunal trophic structure changes during extinction cascades may be central for understanding the dynamics of community disassembly [81]. And while these dynamics may arise naturally from the energetic limitations of mammalian interactions, it may be that the added pressure of subsidized harvest, particularly on megafauna, inevitably leads to collapse.

Acknowledgments

We would like to thank Irina Birskis-Barros, Uttam Bhat, Jessica Blois, Nathaniel Fox, Jacquelyn Gill, Paulo Guimarães Jr., Emily Lindsey, Mathias Pires, Megha Suswaram, and Ritwika VPS for insightful comments and discussions that greatly improved the ideas and concepts that contributed to this manuscript. These ideas benefited greatly from travel funds provided to JDY from the Santa Fe Institute. This project was supported by National Science Foundation grant EAR-1623852 to JDY.

Statement of Authorship

JDY, CPK, and TR conceived of the model. JDY and TR developed the code and oversaw model analysis. All authors reviewed and edited the writing at all stages of composition.

Data and Code Availability

Code and data archived on Zenodo: <https://doi.org/10.5281/zenodo.8213158>

-
- [1] Alonzo, S. H. 2002. State-dependent habitat selection games between predators and prey: the importance of behavioural interactions and expected lifetime reproductive success. *Evol. Ecol. Res.* 4:759–778.
- [2] Alroy, J. 2001. A multispecies overkill simulation of the end-pleistocene megafaunal mass extinction. *Science* 292:1893–1896.
- [3] Barnes, C., D. Maxwell, D. C. Reuman, and S. Jennings. 2010. Global patterns in predator–prey size relationships reveal size dependency of trophic transfer efficiency. *Ecology* 91:222–232.
- [4] Bhat, U., C. P. Kempes, and J. D. Yeakel. 2020. Scaling the risk landscape drives optimal life-history strategies and the evolution of grazing. *Proceedings of the National Academy of Sciences* 117:1580–1586.
- [5] Bradshaw, C. J., C. N. Johnson, J. Llewelyn, V. Weisbecker, G. Strona, and F. Saltr . 2021. Relative demographic susceptibility does not explain the extinction chronology of sahu’s megafauna. *Elife* 10:e63870.
- [6] Brook, B. W., and D. M. J. S. Bowman. 2005. One equation fits overkill: why allometry underpins both prehistoric and modern body size-biased extinctions. *Population Ecology* 47:137–141.
- [7] Brook, B. W., N. S. Sodhi, and C. J. Bradshaw. 2008. Synergies among extinction drivers under global change. *Trends in ecology & evolution* 23:453–460.
- [8] Brose, U., L. Cushing, E. L. Berlow, and T. Jonsson. 2005. Body sizes of consumers and their resources. *Ecology* .
- [9] Burness, G. P., J. Diamond, and T. Flannery. 2001. Dinosaurs, dragons, and dwarfs: the evolution of maximal body size. *Proceedings of the National Academy of Sciences* 98:14518–14523.
- [10] Calder III, W. A. 1983. An allometric approach to population cycles of mammals. *J. Theor. Biol.* 100:275–282.
- [11] Carbone, C., and J. L. Gittleman. 2002. A common rule for the scaling of carnivore density. *Science* 295:2273–2276.
- [12] Carbone, C., G. M. Mace, S. C. Roberts, and D. W. Macdonald. 1999. Energetic constraints on the diet of terrestrial carnivores. *Nature* 402:286–288.
- [13] Carbone, C., A. Teacher, and J. M. Rowcliffe. 2007. The Costs of Carnivory. *PLoS Biol* 5:e22.
- [14] Cardillo, M., G. M. Mace, K. E. Jones, J. Bielby, O. R. P.

- Bininda-Emonds, W. Sechrest, C. D. L. Orme, and A. Purvis. 2005. Multiple causes of high extinction risk in large mammal species. *Science* 309:1239–1241.
- [15] Churchill, S. E. 1993. Weapon technology, prey size selection, and hunting methods in modern hunter-gatherers: implications for hunting in the palaeolithic and mesolithic. *Archaeological Papers of the American Anthropological Association* 4:11–24.
- [16] Cruz, L. R., R. L. Muyaert, M. Galetti, and M. M. Pires. 2022. The geography of diet variation in neotropical carnivora. *Mammal Review* 52:112–128.
- [17] Cruz, L. R., and M. M. Pires. 2022. Body mass ratios determine dietary patterns and help predicting predator-prey interactions of neotropical carnivora. *Mammal Research* .
- [18] Damuth, J. 1981. Home range, home range overlap, and species energy use among herbivorous mammals. *Biol. J. Linn. Soc.* 15:185–193.
- [19] ———. 1981. Population density and body size in mammals. *Nature* 290:699–700.
- [20] ———. 1987. Interspecific allometry of population density in mammals and other animals: the independence of body mass and population energy-use. *Biol. J. Linn. Soc.* 31:193–246.
- [21] de Roos, A. M. 2020. 53The impact of population structure on population and community dynamics. *In Theoretical Ecology: concepts and applications*. Oxford University Press.
- [22] DeAngelis, D. 1980. Energy flow, nutrient cycling, and ecosystem resilience. *Ecology* 61:764–771.
- [23] DeLong, J. P. 2020. Detecting the signature of body mass evolution in the broad-scale architecture of food webs. *The American Naturalist* 196:443–453. PMID: 32970468.
- [24] DeLong, J. P., and D. A. Vasseur. 2012. A dynamic explanation of size–density scaling in carnivores. *Ecology* 93:470–476.
- [25] ———. 2012. Size-density scaling in protists and the links between consumer–resource interaction parameters. *J. Anim. Ecol.* 81:1193–1201.
- [26] Dunne, J. A., H. Maschner, M. W. Betts, N. Huntly, R. Russell, R. J. Williams, and S. A. Wood. 2016. The roles and impacts of human hunter-gatherers in North Pacific marine food webs. *Sci. Rep.* 6:1–9.
- [27] Enquist, B. J., A. J. Abraham, M. B. Harfoot, Y. Malhi, and C. E. Doughty. 2020. The megabiota are disproportionately important for biosphere functioning. *Nature communications* 11:1–11.
- [28] Estes, J. A., J. Terborgh, J. S. Brashares, M. E. Power, J. Berger, W. J. Bond, S. R. Carpenter, T. E. Essington, R. D. Holt, J. B. C. Jackson, R. J. Marquis, L. Oksanen, T. Oksanen, R. T. Paine, E. K. Pikitch, W. J. Ripple, S. A. Sandin, M. Scheffer, T. W. Schoener, J. B. Shurin, A. R. E. Sinclair, M. E. Soulé, R. Virtanen, and D. A. Wardle. 2011. Trophic downgrading of planet Earth. *Science* 333:301–306.
- [29] Farlow, J. O. 1993. On the rareness of big, fierce animals; speculations about the body sizes, population densities, and geographic ranges of predatory mammals and large carnivorous dinosaurs. *American Journal of Science* 293:167.
- [30] Fordham, D. A., S. C. Brown, H. R. Akçakaya, B. W. Brook, S. Haythorne, A. Manica, K. T. Shoemaker, J. J. Austin, B. Blonder, J. Pilowsky, et al. 2022. Process-explicit models reveal pathway to extinction for woolly mammoth using pattern-oriented validation. *Ecology letters* 25:125–137.
- [31] Geiser, F. 1998. Evolution of daily torpor and hibernation in birds and mammals: importance of body size. *Clinical and experimental pharmacology and physiology* 25:736–740.
- [32] Gross, T., L. Rudolf, S. A. Levin, and U. Dieckmann. 2009. Generalized models reveal stabilizing factors in food webs. *Science* 325:747–750.
- [33] Hatton, I. A., K. S. McCann, J. M. Fryxell, T. J. Davies, M. Smerlak, A. R. E. Sinclair, and M. Loreau. 2015. The predator-prey power law: Biomass scaling across terrestrial and aquatic biomes. *Science* 349:aac6284–aac6284.
- [34] Hayward, M. 2006. Prey preferences of the spotted hyaena (*Crocuta crocuta*) and degree of dietary overlap with the lion (*Panthera leo*). *J. Zoology* 270:606–614.
- [35] Hayward, M., P. Henschel, J. O’Brien, M. Hofmeyr, G. Balme, and G. I. Kerley. 2006. Prey preferences of the leopard (*panthera pardus*). *Journal of Zoology* 270:298–313.
- [36] Hayward, M., M. Hofmeyr, J. O’Brien, and G. I. Kerley. 2006. Prey preferences of the cheetah (*acinonyx jubatus*)(felidae: Carnivora): morphological limitations or the need to capture rapidly consumable prey before kleptoparasites arrive? *Journal of Zoology* 270:615–627.
- [37] Hayward, M. W., and G. Kerley. 2008. Prey preferences and dietary overlap amongst Africa’s large predators. *S. African J. Wild. Res.* 38:93–108.
- [38] Hayward, M. W., and G. I. Kerley. 2005. Prey preferences of the lion (*panthera leo*). *Journal of zoology* 267:309–322.
- [39] Hayward, M. W., J. O’Brien, M. Hofmeyr, and G. I. Kerley. 2006. Prey preferences of the african wild dog *lycaon pictus* (canidae: Carnivora): ecological requirements for conservation. *Journal of Mammalogy* 87:1122–1131.
- [40] Hennemann, W. W. 1983. Relationship among body mass, metabolic rate and the intrinsic rate of natural increase in mammals. *Oecologia* 56:104–108.
- [41] Holliday, J., and S. Stepan. 2004. Evolution of hypercarnivory: the effect of specialization on morphological and taxonomic diversity. *Paleobiology* 30:108.
- [42] Horton, D. R., and R. V. Wright. 1981. Cuts on lancefield bones: carnivorous thylacoleo, not humans, the cause. *Archaeology in Oceania* 16:73–80.
- [43] Hou, C., W. Zuo, M. E. Moses, W. H. Woodruff, J. H. Brown, and G. B. West. 2008. Energy Uptake and Allocation During Ontogeny. *Science* 322:736–739.
- [44] Johnson, C. N. 2002. Determinants of loss of mammal species during the late quaternary ‘megafauna’ extinctions: life history and ecology, but not body size. *Proceedings of the Royal Society of London. Series B: Biological Sciences* 269:2221–2227.
- [45] Kay, C. E. 2002. False gods, ecological myths, and biological reality. *Wilderness and political ecology: aboriginal influences and the original state of nature*. University of Utah Press, Salt Lake City pages 238–261.
- [46] Kempes, C. P., S. Dutkiewicz, and M. J. Follows. 2012. Growth, metabolic partitioning, and the size of microorganisms. *PNAS* 109:495–500.
- [47] Lindstedt, S. L., and P. J. Schaeffer. 2002. Use of allometry in predicting anatomical and physiological parameters of mammals. *Lab. Anim.* 36:1–19.
- [48] Lucas, J. R., and L. R. Walter. 1991. When should chickadees hoard food? theory and experimental results. *An-*

- imal Behaviour 41:579–601.
- [49] Millar, J., and G. Hickling. 1990. Fasting Endurance and the Evolution of Mammalian Body Size. *Funct. Ecol.* 4:5–12.
- [50] Milner-Gulland, E., and J. Beddington. 1993. The exploitation of elephants for the ivory trade: an historical perspective. *Proceedings of the Royal Society of London. Series B: Biological Sciences* 252:29–37.
- [51] Moses, M. E., C. Hou, W. H. Woodruff, G. B. West, J. C. Nekola, W. Zuo, and J. H. Brown. 2008. Revisiting a Model of Ontogenetic Growth: Estimating Model Parameters from Theory and Data. <http://dx.doi.org.proxy.lib.sfu.ca/10.1086/679735> 171:632–645.
- [52] Murdoch, W. W., C. J. Briggs, and R. M. Nisbet. 2003. *Consumer-resource Dynamics*. Monographs in population biology. Princeton University Press.
- [53] Nakazawa, T. 2017. Individual interaction data are required in community ecology: a conceptual review of the predator–prey mass ratio and more. *Ecological Research* 32:5–12.
- [54] Pawar, S., A. I. Dell, and V. M. Savage. 2012. Dimensionality of consumer search space drives trophic interaction strengths. *Nature* .
- [55] Pires, M. M., P. L. Koch, R. A. Fariña, M. A. de Aguiar, S. F. dos Reis, and P. R. Guimarães Jr. 2015. Pleistocene megafaunal interaction networks became more vulnerable after human arrival. *Proceedings of the Royal Society B: Biological Sciences* 282:20151367.
- [56] Pirt, S. 1965. The maintenance energy of bacteria in growing cultures. *Proc. Roy. Soc. B* 163:224.
- [57] Prates, L., D. Rivero, and S. I. Perez. 2022. Changes in projectile design and size of prey reveals the role of fishtail points in megafauna hunting in south america .
- [58] Riede, J. O., U. Brose, B. Ebenman, U. Jacob, R. Thompson, C. R. Townsend, and T. Jonsson. 2011. Stepping in elton’s footprints: a general scaling model for body masses and trophic levels across ecosystems. *Ecology letters* 14:169–178.
- [59] Ripple, W. J., and B. Van Valkenburgh. 2010. Linking top-down forces to the pleistocene megafaunal extinctions. *BioScience* 60:516–526.
- [60] Robert, A., S. Chantepie, S. Pavard, F. Sarrazin, and C. Teplitsky. 2015. Actuarial senescence can increase the risk of extinction of mammal populations. *Ecological Applications* 25:116–124.
- [61] Roff, D. 1993. *Evolution Of Life Histories: Theory and Analysis*. Springer US.
- [62] Rohr, R. P., H. Scherer, P. Kehrl, C. Mazza, and L.-F. Bersier. 2010. Modeling food webs: Exploring unexplained structure using latent traits. *Am. Nat.* 176:170–177.
- [63] Savage, V. M., J. F. Gillooly, J. H. Brown, G. B. West, and E. L. Charnov. 2004. Effects of Body Size and Temperature on Population Growth. <http://dx.doi.org.proxy.lib.sfu.ca/10.1086/679735> 163:429–441.
- [64] Schubert, K. A., A. S. Boerema, L. M. Vaanholt, S. F. de Boer, A. M. Strijkstra, and S. Daan. 2010. Daily torpor in mice: high foraging costs trigger energy-saving hypothermia. *Biology letters* 6:132–135.
- [65] Sinclair, A. R. E., S. Mduma, and J. S. Brashares. 2003. Patterns of predation in a diverse predator–prey system. *Nature* 425:288–290.
- [66] Smith, C., and O. Reichman. 1984. The evolution of food caching by birds and mammals. *Annual Review of Ecology and Systematics* 15:329–351.
- [67] Smith, F., A. Boyer, J. Brown, and D. Costa. 2010. The Evolution of Maximum Body Size of Terrestrial Mammals. *Science* .
- [68] Smith, F. A., R. E. Elliott Smith, S. K. Lyons, and J. L. Payne. 2018. Body size downgrading of mammals over the late Quaternary. *Science* 360:310–313.
- [69] Sorkin, B. 2008. A biomechanical constraint on body mass in terrestrial mammalian predators. *Lethaia* 41:333–347.
- [70] Ugan, A. 2005. Does size matter? body size, mass collecting, and their implications for understanding prehistoric foraging behavior. *American Antiquity* 70:75–89.
- [71] Van Valkenburgh, B. 1991. Iterative evolution of hypercarnivory in canids (mammalia: Carnivora): evolutionary interactions among sympatric predators. *Paleobiology* 17:340–362.
- [72] van Valkenburgh, B., X. Wang, and J. Damuth. 2004. Cope’s rule, hypercarnivory, and extinction in North American canids. *Science* 306:101.
- [73] Vézina, A. F. 1985. Empirical relationships between predator and prey size among terrestrial vertebrate predators. *Oecologia* 67:555–565.
- [74] Webb, S. 2009. Late quaternary distribution and biogeography of the southern lake eyre basin (sleb) megafauna, south australia. *Boreas* 38:25–38.
- [75] Weitz, J. S., and S. A. Levin. 2006. Size and scaling of predator–prey dynamics. *Ecology letters* 9:548–557.
- [76] West, G. B., J. H. Brown, and B. J. Enquist. 2001. A general model for ontogenetic growth. *Nature* 413:628–631.
- [77] West, G. B., W. H. Woodruff, and J. H. Brown. 2002. Allometric scaling of metabolic rate from molecules and mitochondria to cells and mammals. *Proc. Natl. Acad. Sci. USA* 99 Suppl 1:2473–2478.
- [78] Wroe, S., T. Myers, R. Wells, and A. Gillespie. 1999. Estimating the weight of the pleistocene marsupial lion, thylacoleo carnifex (thylacoleonidae: Marsupialia): implications for the ecomorphology of a marsupial superpredator and hypotheses of impoverishment of australian marsupial carnivore faunas. *Australian Journal of Zoology* 47:489–498.
- [79] Yeakel, J. D., U. Bhat, and S. D. Newsome. 2020. Caching in or falling back at the sevilleta: the effects of body size and seasonal uncertainty on desert rodent foraging. *The American Naturalist* 196:241–256.
- [80] Yeakel, J. D., C. P. Kempes, and S. Redner. 2018. Dynamics of starvation and recovery predict extinction risk and both damuth’s law and cope’s rule. *Nature communications* 9:1–10.
- [81] Yeakel, J. D., M. M. Pires, L. Rudolf, N. J. Dominy, P. L. Koch, P. R. Guimarães Jr, and T. Gross. 2014. Collapse of an ecological network in Ancient Egypt. *Proceedings of the National Academy of Sciences* 111:14472–14477.
- [82] Yodzis, P., and S. Innes. 1992. Body Size and Consumer-Resource Dynamics. *Am. Nat.* 139:1151–1175.

Table I: Model parameters and values/units

Definition	Parameter	Value/Units
Resource		
density	R	g/m^2
reproduction rate	α	9.49×10^{-9} (1/s)
carrying capacity	k	23×10^3 (g/m^2)
energy density	E_d	1.82×10^4 (J/g)
Consumer		
density	C	g/m^2
body mass	M_C	g
timescale of growth from m_1 to m_2	$\tau(m_1, m_2)$	s
reproduction rate	λ_C^{\max}	1/s
yield coefficient	Y_C	$(\text{g/m}^2 C)/(\text{g/m}^2 R)$
maintenance rate	ρ	1/s
natural mortality rate	μ	1/s
starvation rate	σ^{\max}	1/s
harvest rate	h	1/s
Predator		
steady state density ¹	P^*	$P_0 M_P^{-0.88}$ inds/ m^2
body mass	M_P	g
growth rate	λ_P^{\max}	1/s
yield coefficient	Y_P	$(\text{g/m}^2 P)/(\text{g/m}^2 C)$
predation intensity	w	(0,1)
Metabolic normalization constant	B_0	0.047 ($\text{W g}^{-3/4}$)
Energy to synthesize a unit of mass	E_m	5774 (J g^{-1})
Energy stored in a unit of mass	E'_m	7000 (J g^{-1})
Prop. change PPMR intercept ¹	χ_{int}	(-0.99,2)
Prop. change PPMR slope ¹	χ_{slope}	(-0.99,2)
Extinction-inducing harvest rate	h^\dagger	1/s
Extinction-inducing harvest pressure	ψ^\dagger	inds/yr/ A_{CA}

¹PPMR: Predator-Prey Mass Relationship

Appendix A.: NATURAL MORTALITY

The natural mortality rate is obtained by first assuming that the number of surviving individuals in a cohort N follows a Gompertz relationship [2], where

$$N = N_0 \exp\left(\frac{q_0}{q_a} \left(1 - \exp(-q_a t)\right)\right), \quad (\text{A12})$$

given that q_0 is the initial cohort mortality rate, and q_a is the annual rate of increase in mortality, or the actuarial mortality rate. The change in the cohort's population over time then follows

$$\frac{d}{dt}N = -dN, \quad (\text{A13})$$

such that

$$d = -\frac{1}{N} \frac{d}{dt}N. \quad (\text{A14})$$

If t_ℓ is the expected lifetime of the organism, then the average rate of mortality over a lifetime t_ℓ is

$$\begin{aligned} \mu &= \frac{1}{t_\ell} \int_0^{t_\ell} q_0 \exp(q_a t_\ell) \\ &= \frac{q_0}{q_a t_\ell} \left(\exp(q_a t_\ell) - 1\right). \end{aligned} \quad (\text{A15})$$

The cohort mortality rate q_0 , the actuarial mortality rate q_a and the expected lifetime t_ℓ of a mammal with mass M_C all follow allometric relationships, where $q_0 = 1.88 \times 10^{-8} M_C^{-0.56}$ (1/s) and $q_a = 1.45 \times 10^{-7} M_C^{-0.27}$ (1/s) where M_C is in grams. Together, we obtain the allometric relationship

$$\mu(M_C) = \frac{3.21 \times 10^{-8} \left(\exp(0.586 M_C^{0.03}) - 1\right)}{M_C^{0.59}}. \quad (\text{A16})$$

Appendix B.: VARIATIONS IN MODEL PARAMETERS AND ALLOMETRIC RATES

While our framework dictates that plant growth rates and carrying capacities are directly proportional to consumer steady states, we can gain insight into what drives the very large range of observed consumer densities by exploring the observed ranges of α and k in terrestrial systems. We assume an intrinsic growth rate roughly that of grass where $\alpha = 9.45 \times 10^{-9}$ (s⁻¹), whereas observations among terrestrial plants reveal a range in growth rates from 2.81×10^{-10} to 2.19×10^{-8} [16], according with a change in α of roughly 97% lower and 130% higher than the set value. By incorporating this range into the estimated resource growth rate, we observe that we can account for a large portion of consumer steady state densities around the mean density (inner shaded region, Fig. 1, main text). If we additionally adjust the carrying capacity k of the resource to 90% less-than

and 150% more-than the assumed value of 23×10^3 g/m², our framework accounts for nearly the full range of mammalian steady state densities (outer shaded region, Fig. 1, main text). In this context, the upper-boundary of k observed to capture most higher herbivore densities is ca. 34 kg/m², which is on the higher end of estimated live above-ground biomass densities in terrestrial forests such as in Isle Royal and the Allegheny National Forest [5].

Our model's ability to capture the bounds of mammalian densities at low and high productivity invites some speculation into the actual steepness of the mass-density relationship. While the best-fit slope to Damuth's Law is -0.77 we also observe that the steeper relationship given by our framework better captures the boundaries of mass-density data, whereas varying the intercept of the statistical best-fit would not capture the lower-density outer-boundary of larger species. While within-clade mass-density relationships often reveal a shallower slope than if measured across clades [19], it is possible that the absence of data for larger mammals may bias estimates of the slope towards smaller (shallower) values. Mammalian communities have undergone significant anthropogenic restructuring throughout the Holocene such that many larger species are excluded from the mass-density relationship by way of extinction [13], and the greater prevalence of smaller species may introduce size-dependent biases. For example, if species < 100 g are excluded, the empirical mass-density slope steepens from -0.77 to -0.85.

Considering how variations to the underlying energetic parameters driving consumer-resource dynamics alters the expected mass-density relationship may shed light on key constraints shaping mammalian communities. We next explore how variations in the vital rates included in the consumer-resource model modify the expected intercept and slope of the mammalian mass-density relationship. Different vital rates impact the mass-density relationship in three distinct ways, by either *i*) influencing only the mass-density slope, *ii*) influencing only the mass-density intercept, or *iii*) influencing both. Aside from the resource growth rate and carrying capacity, our framework also includes the intrinsic consumer reproductive rate λ_C^{\max} , the consumer yield coefficient Y_C , and the maximum rate of starvation σ^{\max} . We introduce changes to these rates as, for example, $\lambda_C^{\max'} = \lambda_C^{\max}(1 + \chi)$, where $\chi \in (-1, 2)$ represents the proportion increase or decrease of the altered parameter denoted by '. We note that the recovery rate ρ is sufficiently small that alterations do not have an influence on either the consumer mass-density intercept or slope (fig. B1).

Ignoring the effects of ρ , we can more easily intuit analytical expressions of the steady state conditions for both

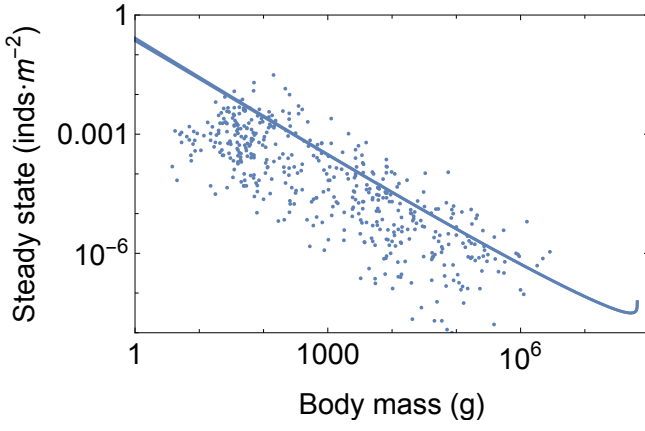


Figure B1: The predicted mass-density relationship with ρ set to its allometric quantity versus $\rho = 0$. The two relationships cannot be distinguished, allowing us to extract insight from the consumer steady state (eq. 7, main text) without its inclusion.

the consumer C and resource R , where

$$C^* = \alpha k Y_C \frac{\sigma^{\max} - 2\lambda_C^{\max} + \sqrt{8\sigma^{\max 2} + (\sigma^{\max} - 2\lambda_C^{\max})^2}}{4\sigma^{\max 2}}$$

$$R^* = k \frac{\sigma^{\max} - 2\lambda_C^{\max} + \sqrt{8\sigma^{\max 2} + (\sigma^{\max} - 2\lambda_C^{\max})^2}}{4\sigma^{\max}}$$
(A17)

We thus observe that the consumer steady state can also be expressed as

$$C^* = \frac{\alpha}{\sigma^{\max}} Y_C R^*. \quad (\text{A18})$$

We discuss how the specific mass-scalings of the relationships impacting the steady states provide more intuition into Damuth's mass-density relationship in the main text.

We can gain additional insight into the role of each vital rate by exploring their quantitative effects on the mass-density relationship directly. Changes to the starvation rate have a large effect on both the consumer-density intercept and slope (Figs. B2,B3). We observe that decreasing σ^{\max} from the expected value ($\chi < 0$) serves to increase the steady state intercept, while decreasing the mass-density slope. By comparison, increasing σ from the expected value ($\chi > 0$) has less effect on the mass-density relationship. In the consumer-resource model described in Eq. 2.3 (main text), starvation is the primary source of consumer mortality, and therefore plays an out-sized role in determining consumer steady states. As this mortality is reduced, consumer densities increase, raising the intercept. However, as consumer starvation rates decline we observe a steeper mass-density slope. Reduced starvation rates therefore principally benefit the steady state densities of smaller species, with reduced effects observed for larger-bodied mammals. Because fat biomass scales super-linearly with body mass (see Table 1, main text), the populations of larger consumers are more resilient to the effects of starvation, whereas those of smaller consumers are more prone.

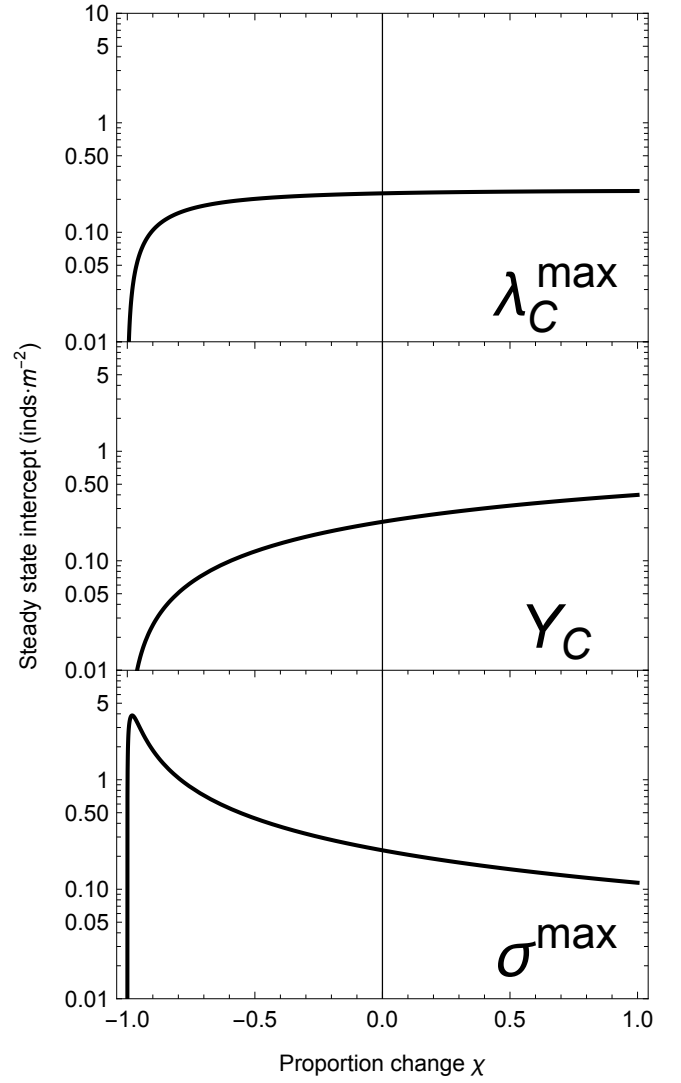


Figure B2: The effects of changes to metabolic parameters on the prediction of the mass-density relationship.

The consumer's maximal rate of reproduction λ_C^{\max} influences only the mass-density slope except for the case $\chi \rightarrow -1$, where growth becomes zero. Above this trivial limit, we observe the consumer growth rate to have a negative effect on the mass-density slope, such that as the growth rate increases, the mass-density relationship becomes steeper (Figs. B2,B3). As the intercept does not change, this means that the steady states of larger-bodied consumers decline with increasing λ_C^{\max} , while those of smaller-bodied consumers remain unaltered, though the effect is slight. Of more interest is the effect of the yield coefficient Y_C and starvation rate σ^{\max} (Figs. B2,B3). The yield coefficient represents the conversion of resources to consumer biomass, where an increase in χ correlates to large increases in consumer steady state without altering the mass-density slope. Here we observe that increased efficiency in converting resource to consumer biomass will have an effect similar to increasing

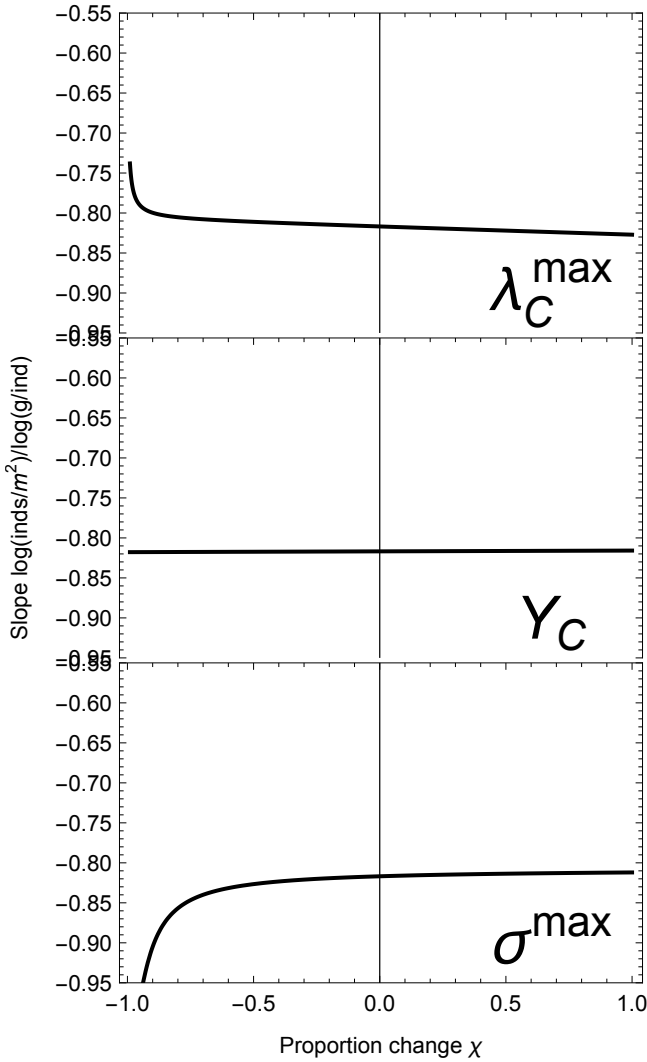


Figure B3: The effects of changes to metabolic parameters on the prediction of the mass-density relationship.

resource productivity, as the effective abundance of the resource is greater when relatively fewer resources fuel a given unit of consumer biomass. Because $Y_C \propto E_d$, where E_d is the energy density of the resource (see methods), resource quality is therefore expected to translate directly to higher consumer steady state densities.

Appendix C.: MORTALITY FROM PREDATION

Per-capita mortality rate from predation The per-capita mortality rate from predation of the herbivore consumer with mass M_C and population density C by a mammalian predator with body mass M_P and population density P is given by

$$\beta(C, P) = w \frac{\lambda_P(C)P}{CY_P}, \quad (\text{A19})$$

where $\lambda_P(C)$ is the growth rate of the predator, Y_P is the predator yield coefficient, describing the grams of predator produced per gram of prey consumed, and w is the degree of predation intensity ($w = 1$ denotes high predation intensity, whereas $w < 1$ denotes lower predation intensity). Assuming a linear functional response for predation mortality, $\lambda_P(C)$ is maximized to λ_P^{\max} when the consumer reaches its theoretical maximum population density, which we calculate by converting the resource carrying capacity directly to grams of consumer produced, or $C^{\max} = Y_C k$. The growth rate of the predator is then given by

$$\lambda_P(C) = \lambda_P^{\max} \frac{C}{C^{\max}} = \lambda_P^{\max} \frac{C}{Y_C k}. \quad (\text{A20})$$

Together, we observe the per-capita mortality rate to be (as expected) independent of the consumer density C , and is simplified to

$$\beta(P) = w \frac{\lambda_P^{\max} P}{Y_P Y_C k}, \quad (\text{A21})$$

where we assume that the predator population remains at empirically measured steady state densities for mammalian carnivores, where $P \equiv P^* = P_0 M_P^{-0.88}$ [3]. This assumption is required because the effects of predation are implicit rather than explicit, and effectively assumes that predator populations operating far below this relationship are not viable. While there is bound to be a range of viable densities for a predator of a given body size, that mass-density relationships exist at all indicates that population densities are highly constrained over evolutionary time and therefore represent a predator energetic demand as a function of body size. Accordingly, if the predator mass-density relationship P^* represents an expected energetic requirement for a functioning predator population, our assumption of predation as a constant, rather than dynamic, influence on herbivore mortality reveals the dynamic consequence of such energetic relationships. We suggest that it is these energetic mismatches that may constrain longer-timescale macroevolutionary forces, even if the shorter-timescale ecological dynamics may be more idiosyncratic and complex than our minimal model captures.

Herbivore and predator yields As described in the main text, consumer yield is calculated

$$Y_C = \frac{M_C E_d}{\int_0^{t_{\lambda_C}} B_0 m(t)^\eta dt}, \quad (\text{A22})$$

where E_d is the energy density of the plant resource R (Joules/g) and the denominator is the lifetime energy use required by the herbivore consumer to reach maturity (Joules). The parameters t_{λ_C} and B_0 are the timescale associated with reaching reproductive maturity and the metabolic coefficient for herbivorous mammals, respectively, and $\eta = -3/4$ is the metabolic exponent (see Table

1, main text). The predator yield is calculated similarly, where

$$Y_P = \frac{M_C E_C}{\int_0^{t_{\lambda_P}} B_{0P} m(t)^\eta dt}, \quad (\text{A23})$$

where E_C is the energy density of the herbivore being consumed, and the denominator is the lifetime energy use required by the predator to reach maturity. The parameters t_{λ_P} and B_{0P} are the timescale associated with reaching reproductive maturity and the metabolic coefficient for predatory mammals, respectively, and $\eta = -3/4$ is the metabolic exponent. We note that the metabolic coefficient for predators is different than that for mammals [18].

The energy density of herbivore consumers changes with body mass M_C . For example, small mammals have very low percent body fat, whereas very large mammals have high percent body fat. We assume that predators consume all non-skeletal mass of prey. Because the amount of consumable tissues with different energy densities within an herbivore varies allometrically, so too should the energy density E_C . We consider four primary tissue groups: a consumable set composed of muscle, fat, and *other* tissues, and an non-consumable set composed only of skeletal tissues. If the scalings associated with fat, muscle, and skeletal tissues are $M_C^{\text{fat}} = f_0 M_C^{1.19}$, $M_C^{\text{musc}} = g_0 M_C^{1.00}$, and $M_C^{\text{skel}} = h_0 M_C^{1.09}$ [with normalization constants $f_0 = 0.02$, $g_0 = 0.38$, and $h_0 = 0.0335$; 20], the scaling of the *other* tissue (gut tissue, organ tissue, etc) is given by $M_C^{\text{other}} = M_C - (M_C^{\text{fat}} + M_C^{\text{musc}} + M_C^{\text{skel}})$. The energy density of fat is $E_{\text{fat}} = 37700$ J/g, whereas the energy density of muscle is $E_{\text{musc}} = 17900$ J/g [15]. If we assume that gut and organ tissues have roughly the same energy density as muscle, the attainable energy density for an herbivore of size M_C is given by

$$E_C(M_C) = E_{\text{fat}} \frac{M_C^{\text{fat}}}{M_C} + E_{\text{musc}} \left(\frac{M_C^{\text{musc}}}{M_C} + \frac{M_C^{\text{other}}}{M_C} \right). \quad (\text{A24})$$

Large-bodied Predator-Prey Mass Relationship (PPMR) The predator growth rate λ_P^{max} , the time required for the predator to reach reproductive maturity t_{λ_P} , and the predator's steady state population density P^* are allometric relationships that depend on predator body mass M_P . Accordingly, for an herbivore of a given mass M_C , we must anticipate the size of its likely predator M_P . This is very different than the predator-centric perspective of anticipating the average prey size for a given predator [4]. For example, the most preferred prey mass for an African lion is ca. 350 kg [11], where the inclusion of megaherbivores to diet is comparatively low. However from a megaherbivore's perspective, lions may represent the only potential predator. In other words, because the range of prey body mass increases for predators of larger body mass [21], it is the upper limit of the range that impacts the populations of larger herbivores.

To obtain an herbivore-centric measure of the expected predator mass given a particular herbivore mass $E\{M_P|M_C\}$, we first compiled the known diets of large-bodied predators, including tigers, lions, hyenas, leopards, dhole, wild dogs, and cheetahs [7–12]. Because smaller mammalian predators and prey have very different PPMRs than larger-bodied mammalian predators and prey, we here focus exclusively on the predators of large-bodied herbivore prey $> 10^5$ g. From the mean proportional reliance of predators on large-bodied prey [7–12], we repeatedly sampled predator dietary distributions to reflect each predator's reliance as a function of prey mass. We introduced variability in predator and prey masses by assuming that body sizes were normally distributed about the expected value with a standard deviation of $\pm 25\%$, allowing us to obtain a distribution of expected predator diets as a function of prey mass. From this relationship, we then evaluated the expected predator mass for a given prey mass range to obtain $E\{M_P\}$ (Fig. 4b, main text), demonstrating the allometric relationship of $E\{M_P\} = 9.76 \times 10^3 M_C^{0.21}$, where we used the output of 100 independent replicates to robustly estimate the best fit. We emphasize that this relationship only pertains to large-bodied predators and prey $> 10^5$ g. Alterations to and variations from this relationship are explored in the main text.

Including the empirically-measured PPMR (or a variant of the empirically measured PPMR – see below) results in the appearance of a transcritical bifurcation at consumer mass M_C^\dagger . We observe that this critical mass threshold results in the extinction of the consumer population characterized by body sizes $M_C \geq M_C^\dagger$ (fig. C1A). At this body mass, the Determinant of the Jacobian matrix characterizing the system presented in eq. 3 (main text) with predation mortality included (eq. 8, main text) is zero (fig. C1B), aligning with the real component of a single eigenvalue crossing zero and becoming positive (fig. C1C). While we do not derive a normal form for this bifurcation, these features strongly suggest the observed bifurcation is transcritical in nature [14].

As explored in the main text, the empirically-measured PPMR for large-bodied mammals results in a threshold body size for herbivore consumers M_C^\dagger . This size marks the point where the predator population, with a body mass derived from the PPMR, cannot sustain its own growth from the predated herbivore population, thereby driving the herbivore population to extinction. The size at which M_C^\dagger occurs is both dependent on the nature of the PPMR, as well as predation intensity w . As predation intensity w decreases, M_C^\dagger increases (Fig. C2).

By allowing the PPMR to vary as

$$E\{M_P\} = v_0(1 + \chi_{\text{int}})M_C^{v_1(1 + \chi_{\text{slope}})}, \quad (\text{A25})$$

where the proportional changes in the PPMR intercept and slope are given by χ_{int} and $\chi_{\text{slope}} \in (-0.99, 2)$, so does the threshold herbivore body mass M_C^\dagger and, by extension, the related threshold predator body mass M_P^\dagger .

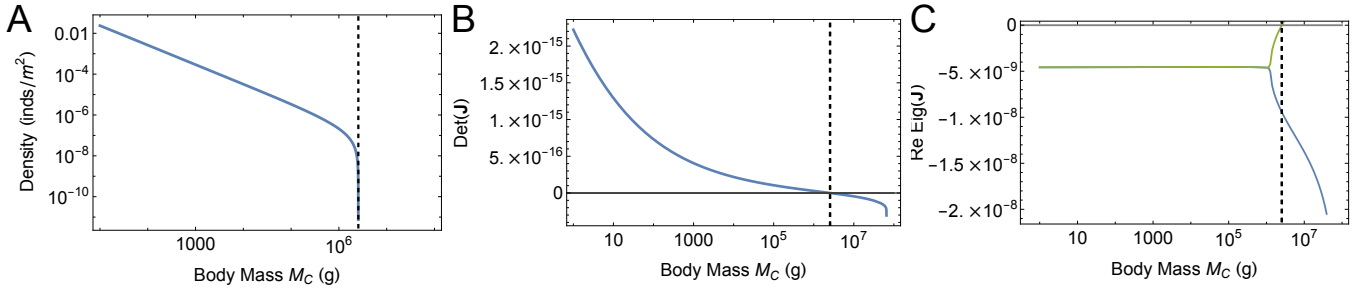


Figure C1: A. Consumer population density as a function of mass M_C . B. The determinant of the Jacobian matrix for the system presented in eq. 3 (main text) with predation mortality included (eq. XX, main text) as a function of mass M_C . C. The Real component of the two eigenvalues of the Jacobian assessed in panel B, as a function of mass M_C . The dashed line in each panel is the measured consumer mass threshold $M_C^\dagger = 2.5 \times 10^6$ g. The Gray horizontal line in panels B,C denotes zero on the y-axis.

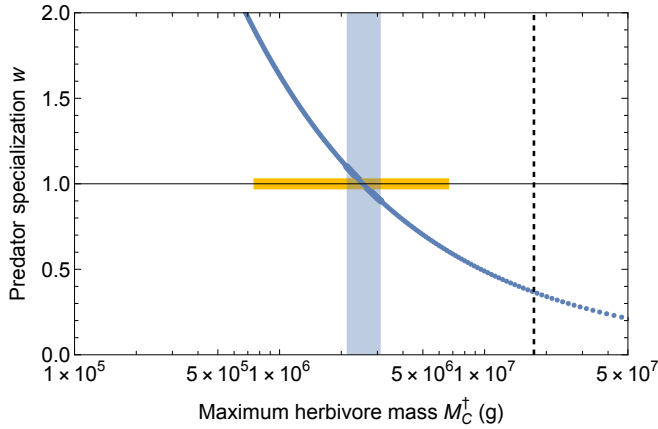


Figure C2: The effect of changing the predation intensity w on the single herbivore consumer population. If $w = 1$, predation intensity is maximized, is lower if $0 < w < 1$, and is above the maximal level required to support a predator population if $w > 1$. The blue region denotes herbivore threshold mass range characterizing $w = 1 \pm 0.1$. The yellow line denotes the mass range of contemporary elephantids. Vertical dashed line denotes the size of the largest terrestrial mammal (*Deinotherium* at ca. 1.74×10^7 , corresponding to $w = 0.37$, such that predation intensity is moderate.

From Fig. 4D (main text), we observe that changing the intercept and slope of the PPMR has a large influence on M_C^\dagger and M_P^\dagger . Across this range of potential PPMRs, we highlight those values for the intercept and slope of the PPMR that permit megatrophic interactions, where both megapredators subsist on megaherbivores at the threshold body mass (highlighted region in Fig. 4D, main text). Fig. C3 shows the relationship between megapredator and megaherbivore body masses highlighted within this region. Allowing both the PPMR to vary and assuming lower predation intensity ($w = 0.37$) enables much larger body sizes for megaherbivores and their associated megapredators (Fig. C4).

Finally, we note that changes to both the resource growth rate α as well as to the resource carrying capacity k can impact the consumer size at which populations become infeasible M_C^\dagger . Because the consumer steady state

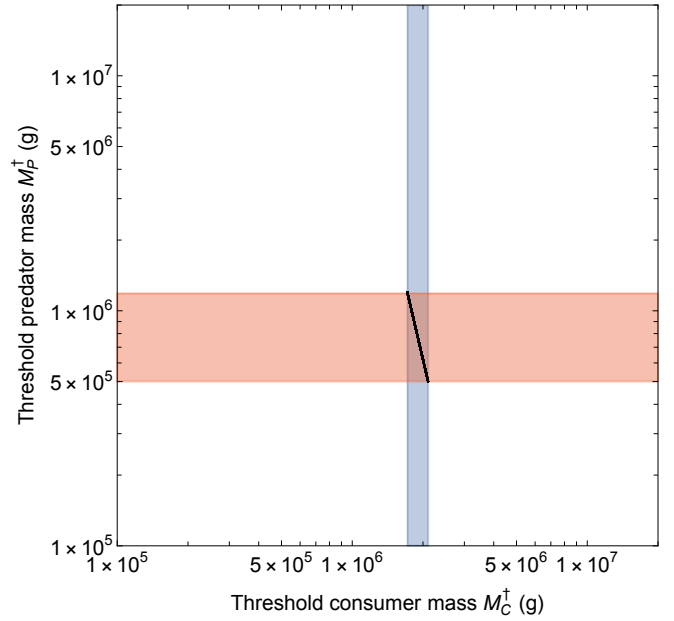


Figure C3: Mass ranges corresponding to feasible megatrophic interactions (where herbivore and predator threshold masses are $> 5 \times 10^5$ g) across variations to the assumed PPMR, demarcated by the white bands in Fig. 4C,D (main text), and assuming high predation intensity ($w = 1$).

is directly proportional to both of these parameters (see eq. 7, main text), a lower growth rate and/or carrying capacity lowers the intercept of the steady state mass-density relationship $C^*(M_C)$. Analysis of the effect of changes to k (and this will be the same for α) reveals that while it has influence on M_C^\dagger , it is not incredibly large (Fig. C5). However this relationship carries with it an important message: in environments with lower carrying capacities and/or plant growth rates, we would expect a lower mass threshold bounding feasible megaherbivore populations.

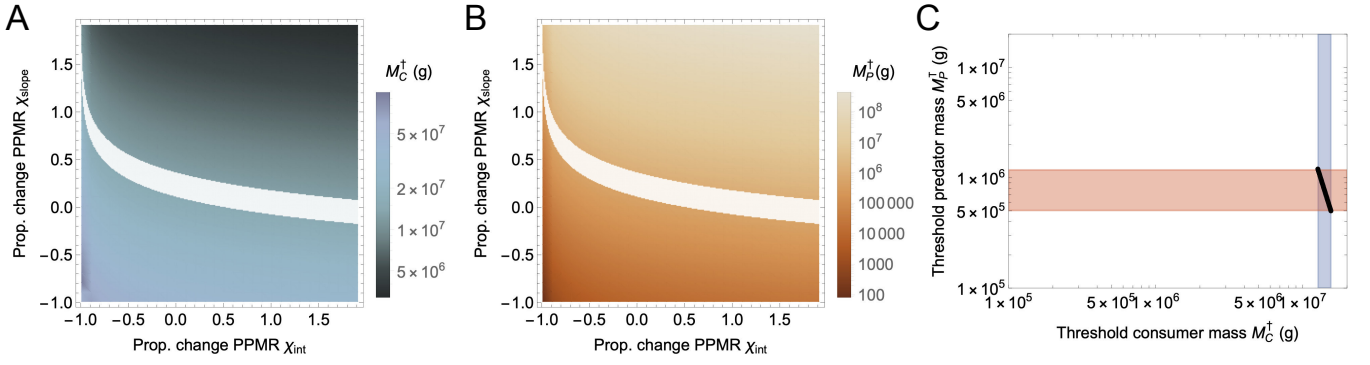


Figure C4: The effects of lower predation intensity ($w = 0.37$) on A. threshold herbivore mass M_C^\dagger and B. threshold predator mass M_P^\dagger across variable PPMRs, where $E\{M_P\} = v_0(1 + \chi_{\text{int}})M_C^{v_1(1 + \chi_{\text{slope}})}$ and both χ_{int} and $\chi_{\text{slope}} \in (-0.99, 2)$, and $v_0 = 9.76 \times 10^3$ and $v_1 = 0.21$ are set as in the main text. White bands denote regions of χ_{int} and χ_{slope} where megatrophic interactions are feasible (i.e. both predator and herbivore threshold masses are $> 5 \times 10^5$ g). C. Mass ranges corresponding to feasible megatrophic interactions in the white bands in A. and B.

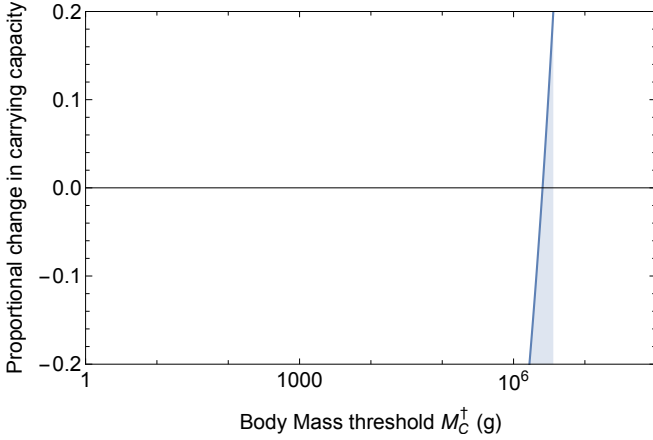


Figure C5: The effect of an altered carrying capacity k on the consumer mass threshold M_C^\dagger . Carrying capacity values that vary from -20% to +20% give rise to an M_C^\dagger roughly 65% and 140% the original estimated mass of 2.55×10^6 g. Equivalent variations in α will result in the same changes to M_C^\dagger given its role in eq. 7 (main text). The shaded region highlights the mass range captured by the altered carrying capacity.

Appendix D: DERIVATION OF HARVESTING MORTALITY

We first determined the harvest rate $h = h^\dagger$ required to drive an herbivore population to extinction, thereby satisfying the condition $C^*(M_C|h) = 0$ as a function of herbivore body mass M_C . This extinction-inducing harvest rate, itself now a function of consumer body mass $h^\dagger(M_C)$, defines the rate at which the population must be harvested to drive the steady state to zero. To compare this rate against measures of harvest both in nature and predicted from other mathematical or computational treatments of harvest-induced extinction, we calculated the harvest pressure ψ^\dagger , which we defined as the number of herbivore individuals per area harvested at this

rate to reduce the population to some proportion ϵ of its steady state. This harvest pressure is thus defined by some number of individuals harvested per year over a certain number of years to reduce the population from C^* to its post-harvest density ϵC^* .

To calculate harvest pressure, we first assume that at the steady state, harvest is occurring on a shorter-than-generational timescale. For megaherbivores such as elephants, a generation is roughly 25 years [23], and for harvest pressures that must be applied beyond this period of time, we would expect population growth to counter the negative effects of harvest. Assuming harvest-only change, we simplify the dynamics to

$$\frac{d}{dt}C = -h^\dagger(M_C)C, \quad (\text{A26})$$

where the time to reduce C^* to ϵC^* is

$$\begin{aligned} C(t) &= C_0 e^{-h^\dagger(M_C)t}, \\ \epsilon C^* &= C^* e^{-h^\dagger(M_C)t} \\ t_\epsilon &= -\frac{\log(\epsilon)}{h^\dagger(M_C)}. \end{aligned} \quad (\text{A27})$$

We note that for elephant-sized herbivores and larger, $t_\epsilon \leq 23$ years. While the time required to harvest the population to ϵC^* is only just approaching generational timescales, it should be treated as a minimum t_ϵ given the effects of population growth will prolong the imposed harvest effort. Harvest pressure is then calculated as

$$\psi^\dagger = \frac{C^*(1 - \epsilon)}{M_C t_\epsilon} c_0 = -h^\dagger(M_C) \frac{C^*(1 - \epsilon)}{M_C \log(\epsilon)} c_0 \quad (\text{A28})$$

where the constant c_0 denotes the conversion from inds/m²/second to inds/A_{CA}/year, where $A_{CA} = 4.24 \times 10^{11}$ m² is the arbitrarily-chosen area of California. This conversion is particularly important for evaluating other harvest measures from the

historical record and estimates from independent models and simulations for extinct species. As described in the main text, the extinction-inducing harvest pressure is calculated to be 4.3×10^3 inds/yr/ A_{CA} for an elephant-sized organism of $M_C = 2.5 \times 10^6$ g (see Fig 5, main text).

Harvest pressure on Pleistocene mammoths We compare our measure of harvest pressure to that calculated for mammoths (*Mammuthus primigenius*) by Fordham et al. [6]. Because Fordham et al. [6] employ a much more specific and detailed assessment of the effects of harvest specifically for mammoths over a spatially explicit landscape, we must make a few simplifications in order to derive a comparable estimate. First, the harvest interaction between mammoth populations and humans is modeled as a Type II functional response, where, again isolating population-level effects to that of harvest we obtain

$$\frac{d}{dt}C = -\frac{sNFC}{G + \frac{C}{C_{\max}M_C}}, \quad (\text{A29})$$

where N is the normalized human population density maximized at unity, the constant $s = 7.884 \times 10^{-8}$ generations/second (where a generation is 25 years), F represents the effectiveness of human hunting, ranging from (0.01, 0.34), $C_{\max} = 1.875 \times 10^{-6}$ g/m² is the maximum mammoth population density (converted from the average degree-by-degree grid cells in Siberia), $G = 0.4$ is the half-saturation constant, and $M_C = 2.5 \times 10^6$ grams.

Solving for the time required to reduce the population to ϵC^* , we obtain

$$t_{\epsilon}^{\text{mammoth}} = \frac{C^* - C_{\max}GM_C \log \left[C^* \exp\left(\frac{C^*\epsilon}{C_{\max}GM_C}\right)\epsilon \right]}{sC_{\max}FM_CN}. \quad (\text{A30})$$

We then calculate the harvest pressure as

$$\psi^{\text{mammoth}} = c_0 \frac{sC_{\max}FN(C^* - C^*\epsilon)}{C^* - C_{\max}GM_C \log \left[C^* \exp\left(\frac{C^*\epsilon}{C_{\max}GM_C}\right)\epsilon \right]}, \quad (\text{A31})$$

where the constant c_0 again denotes the conversion from inds/m²/second to inds/ A_{CA} /year, where A_{CA} is the arbitrarily-chosen area of California. Given a range in $F \in (0.01, 0.35)$ and $N \in (0.01, 1)$, we obtain a distribution of values for mammoth harvest pressure with a median value of 1.24×10^4 inds/yr/ A_{CA} over the course of 9.8 years. The bounds of the estimated range from 5×10^4 inds/yr/ A_{CA} over the course of 2 years to 5×10^2 inds/yr/ A_{CA} over the course of ca. 200 years (the range is plotted as the vertical black line in Fig. 5, main text).

Harvest pressure on Pleistocene *Diprotodon* The harvest rate needed to collapse *Diprotodon* populations was calculated by Bradshaw et al. [1], where a harvest pressure of between 400-500 inds/year/area of Australia was sufficient to collapse the population. Translating

this to the area of California, we obtain between 678 to 848 inds/yr/ A_{CA} , with a mean of 763.2 inds/yr/ A_{CA} .

Harvest pressure on historical elephants *Loxodonta africana* Elephant harvest rates are estimated from historical documentation of the ivory trade detailed in Milner-Gulland and Beddington [17]. While the trade volume oscillates with changes in technology, access to habitats within Africa, and the feedbacks of trade on elephant population size, we compare our results against estimates taken at two points in time: early in the ivory trade (1810), and late in the ivory trade (1987). From Milner-Gulland and Beddington [17] we assume that each elephant killed contributes 1.88 tusks, and that tusk mass begins at 15 kg per tusk early in trade to 5 kg per tusk in later years. While the area from which elephants were harvested is largely unknown, we assume the area harvested is that assessed to be suitable elephant habitat in sub-Saharan Africa, estimated at 3.22×10^{12} m² [22]. From rates of ca. 1×10^5 kg/yr of ivory harvested in 1810 to ca. 9.7×10^5 kg/yr of ivory harvested in 1987, normalized to habitat area and converted to the area of California, we obtain estimates of ca. 467 inds/yr/ A_{CA} in 1810 to ca. 1.33×10^4 inds/yr/ A_{CA} in 1987 (see Fig. 5, main text).

-
- [1] Bradshaw, C. J., C. N. Johnson, J. Llewelyn, V. Weisbecker, G. Strona, and F. Saltr e. 2021. Relative demographic susceptibility does not explain the extinction chronology of sahur’s megafauna. *Elife* 10:e63870.
- [2] Calder III, W. A. 1983. An allometric approach to population cycles of mammals. *J. Theor. Biol.* 100:275–282.
- [3] Carbone, C., and J. L. Gittleman. 2002. A common rule for the scaling of carnivore density. *Science* 295:2273–2276.
- [4] Carbone, C., G. M. Mace, S. C. Roberts, and D. W. Macdonald. 1999. Energetic constraints on the diet of terrestrial carnivores. *Nature* 402:286–288.
- [5] De Jager, N. R., P. J. Drohan, B. M. Miranda, B. R. Sturtevant, S. L. Stout, A. A. Royo, E. J. Gustafson, and M. C. Romanski. 2017. Simulating ungulate herbivory across forest landscapes: A browsing extension for landis-ii. *Ecological Modelling* 350:11–29.
- [6] Fordham, D. A., S. C. Brown, H. R. Ak akaya, B. W. Brook, S. Haythorne, A. Manica, K. T. Shoemaker, J. J. Austin, B. Blonder, J. Pilowsky, et al. 2022. Process-explicit models reveal pathway to extinction for woolly mammoth using pattern-oriented validation. *Ecology letters* 25:125–137.
- [7] Hayward, M. 2006. Prey preferences of the spotted hyaena (*Crocuta crocuta*) and degree of dietary overlap with the lion (*Panthera leo*). *J. Zoology* 270:606–614.
- [8] Hayward, M., P. Henschel, J. O’Brien, M. Hofmeyr, G. Balme, and G. I. Kerley. 2006. Prey preferences of the leopard (*panthera pardus*). *Journal of Zoology* 270:298–313.
- [9] Hayward, M., M. Hofmeyr, J. O’Brien, and G. I. Kerley. 2006. Prey preferences of the cheetah (*acinonyx jubatus*)(felidae: Carnivora): morphological limitations or the need to capture rapidly consumable prey before kleptoparasites arrive? *Journal of Zoology* 270:615–627.
- [10] Hayward, M. W., and G. Kerley. 2008. Prey preferences and dietary overlap amongst Africa’s large predators. *S. African J. Wild. Res.* 38:93–108.
- [11] Hayward, M. W., and G. I. Kerley. 2005. Prey preferences of the lion (*panthera leo*). *Journal of zoology* 267:309–322.
- [12] Hayward, M. W., J. O’Brien, M. Hofmeyr, and G. I. Kerley. 2006. Prey preferences of the african wild dog *lycaon pictus* (canidae: Carnivora): ecological requirements for conservation. *Journal of Mammalogy* 87:1122–1131.
- [13] Koch, P. L., and A. Barnosky. 2006. Late Quaternary extinctions: state of the debate. *Annu. Rev. Ecol. Evol. Syst.* 37:215–250.
- [14] Kuznetsov, Y. 1998. *Elements of Applied Bifurcation Theory*. Springer, New York.
- [15] Merrill, A., and B. Watt. 1973. Part 2: digestibility and available energy of foods. *Energy value of foods: basis and derivation. Agriculture handbook No 74*:8–24.
- [16] Michaletz, S. T., D. Cheng, A. J. Kerkhoff, and B. J. Enquist. 2014. Convergence of terrestrial plant production across global climate gradients. *Nature* 512:39–43.
- [17] Milner-Gulland, E., and J. Beddington. 1993. The exploitation of elephants for the ivory trade: an historical perspective. *Proceedings of the Royal Society of London. Series B: Biological Sciences* 252:29–37.
- [18] Mu oz-Garcia, Agust  and Williams, Joseph B. 2005. Basal metabolic rate in carnivores is associated with diet after controlling for phylogeny. *Physiological and Biochemical Zoology* 78:1039–1056. PMID: 16228943.
- [19] Pedersen, R.  ., S. Faurby, and J.-C. Svenning. 2017. Shallow size–density relations within mammal clades suggest greater intra-guild ecological impact of large-bodied species. *J. Anim. Ecol.* 86:1205–1213.
- [20] Prange, H. D., J. F. Anderson, and H. Rahn. 1979. Scaling of skeletal mass to body mass in birds and mammals. *The American Naturalist* 113:103–122.
- [21] Sinclair, A. R. E., S. Mduma, and J. S. Brashares. 2003. Patterns of predation in a diverse predator–prey system. *Nature* 425:288–290.
- [22] Thouless, C., H. T. Dublin, J. Blanc, D. Skinner, T. Daniel, R. Taylor, F. Maisels, H. Frederick, and P. Bouch . 2016. African elephant status report 2016. An update from the African Elephant Database .
- [23] Wittemyer, G., D. Daballen, and I. Douglas-Hamilton. 2013. Comparative demography of an at-risk african elephant population. *PloS one* 8:e53726.